Table S1 The mean bias (±s.d.) and RMSE of the simulated CH_4 (CO_2) annual gradient for all the stations and different station groups. Results from both ZASIA and REG are presented. Statistics are given for stations within the zoomed region and outside the zoomed region.

CH_4 (ppb)		All		Marine		Coastal		Mountain		Continental	
		ZASIA	REG	ZASIA	REG	ZASIA	REG	ZASIA	REG	ZASIA	REG
Bias	Zoom	-1.2±13.9	-5.4±20.1	2.8±17.9	-2.1±24.7	-3.1±15.3	-12.3±19.4	2.1±10.1	-3.6±2.0	-8.1±9.4	2.9±31.5
	Non zoom	-8.5±12.2	-9.2±6.4	-3.0±2.1	-4.2±0.2	-5.0±8.4	-11.4±3.7	–	–	-32.0	-19.6
RMSE	Zoom	13.6	20.3	16.3	22.2	14.5	21.7	9.0	4.0	11.2	25.9
	Non zoom	14.0	10.9	3.5	4.2	7.8	11.7	–	–	32.0	19.6
CO_2 (ppm)		All		Marine		Coastal		Mountain		Continental	
		ZASIA	REG	ZASIA	REG	ZASIA	REG	ZASIA	REG	ZASIA	REG
Bias	Zoom	0.3±2.4	0.0±2.5	0.0±1.5	0.1±1.3	1.4±3.0	0.3±3.3	-0.7±3.7	-0.9±3.9	0.0±1.1	0.3±1.7
	Non zoom	-1.2±2.4	-0.5±1.9	-0.6±0.2	-0.5±0.0	-0.8	-1.7	–	–	-1.9±3.9	-0.1±3.1
RMSE	Zoom	2.4	2.5	1.3	1.1	3.1	3.1	3.3	3.5	1.0	1.6
	Non zoom	2.5	1.8	0.6	0.5	0.8	1.7	–	–	3.7	2.5

Table S2 The correlation between the simulated and observed CH_4 diurnal cycles for stations that have continuous CH_4 measurements. Correlation coefficients are given for all the sampling days with a complete 24-hour profile and for different months (M1–M12).

		AMY	BKT	COI	GSN	HAT	HLE	MNM	PON	RYO	YON
All	ZASIA	0.64	0.27	0.53	0.31	0.22	0.35	0.22	0.19	0.20	0.40
	RGL	0.56	-0.12	0.56	0.09	0.03	0.22	0.24	0.21	0.32	0.19
M1	ZASIA	0.66	0.62	0.75	0.60	0.45	0.18	0.45	0.09	0.47	0.19
	RGL	0.50	0.45	0.63	0.52	0.12	-0.21	0.35	0.38	0.23	0.18
M2	ZASIA	0.11	0.16	0.61	0.49	0.17	0.54	0.02	0.05	0.21	0.45
	RGL	0.19	0.16	0.40	0.32	-0.29	0.28	0.36	0.46	0.25	0.00
M3	ZASIA	0.60	0.68	0.74	0.55	0.11	n.a.	0.01	0.27	0.20	0.53
	RGL	0.56	0.39	0.77	0.53	-0.44	n.a.	0.06	0.43	-0.06	0.02
M4	ZASIA	0.50	-0.06	0.67	0.41	-0.10	n.a.	0.45	0.54	0.35	0.48
	RGL	0.43	-0.40	0.61	-0.17	-0.24	n.a.	0.13	0.70	0.48	0.13
M5	ZASIA	0.43	-0.03	0.40	0.57	0.22	n.a.	0.28	0.67	0.38	0.03
	RGL	0.29	-0.54	0.64	-0.04	-0.16	n.a.	0.25	0.58	0.31	-0.09
M6	ZASIA	0.85	-0.37	0.55	0.39	0.15	n.a.	0.26	n.a.	-0.34	0.26
	RGL	0.70	-0.38	0.66	0.15	-0.19	n.a.	0.30	n.a.	-0.16	-0.07
M7	ZASIA	0.64	-0.28	0.67	0.02	0.34	0.82	0.37	n.a.	0.19	-0.12
	RGL	0.53	-0.35	0.72	-0.13	0.12	0.91	0.32	n.a.	0.68	-0.10
M8	ZASIA	0.73	0.25	0.59	0.42	-0.03	0.70	-0.01	0.72	0.51	0.11
	RGL	0.67	-0.49	0.51	0.05	0.24	0.86	0.10	-0.70	0.60	-0.10
M9	ZASIA	0.77	-0.11	0.73	0.12	0.34	-0.12	0.28	0.45	0.39	0.41
	RGL	0.68	-0.29	0.79	-0.08	0.11	-0.75	0.53	0.12	0.44	0.27
M10	ZASIA	0.82	0.29	0.73	0.02	-0.07	0.17	0.11	0.29	0.25	0.34
	RGL	0.73	-0.48	0.68	0.29	0.25	-0.43	-0.15	0.62	0.31	0.27
M11	ZASIA	0.87	0.13	0.32	0.45	0.59	-0.08	0.19	0.02	-0.19	0.65
	RGL	0.85	-0.03	0.34	0.41	0.70	0.33	0.44	0.21	0.10	0.64
M12	ZASIA	0.64	0.28	0.43	-0.04	0.45	0.68	0.22	0.08	0.49	0.71
	RGL	0.62	-0.51	0.48	-0.19	0.27	0.70	0.09	0.08	0.31	0.42

Table S3 The correlation between the simulated and observed CO_2 diurnal cycles for stations that have continuous CO_2 measurements. Correlation coefficients are given for all the sampling days with a complete 24-hour profile and for different months (M1–M12).

		AMY	BKT	DDR	GSN	HLE	KIS	MKW	MNM	PON	RYO	YON
All	ZASIA	0.30	0.23	-0.35	0.17	-0.12	0.79	0.65	0.13	0.33	0.51	-0.05
	RGL	0.19	-0.19	-0.34	0.09	0.16	0.78	0.69	0.13	0.23	0.39	0.32
M1	ZASIA	0.00	0.56	0.63	0.53	-0.36	0.35	0.41	0.41	0.89	0.26	0.01
	RGL	0.15	0.28	0.78	0.25	-0.15	-0.07	0.11	0.37	0.55	0.15	0.36
M2	ZASIA	0.14	0.24	0.65	0.38	-0.19	0.44	0.37	0.22	0.81	0.12	-0.17
	RGL	0.24	-0.10	0.63	0.06	0.07	0.30	0.01	0.03	0.39	0.09	0.44
M3	ZASIA	0.15	0.32	0.37	0.55	-0.03	0.61	0.37	0.13	0.22	0.07	0.06
	RGL	-0.43	-0.19	0.15	0.52	0.06	0.55	0.16	0.28	0.44	-0.47	0.05
M4	ZASIA	0.25	0.39	0.00	0.09	0.25	0.90	0.68	0.33	0.50	0.32	0.21
	RGL	0.10	-0.22	-0.16	-0.14	0.21	0.81	0.47	-0.28	0.67	0.28	0.47
M5	ZASIA	0.03	0.36	-0.58	0.25	0.31	0.82	0.82	-0.15	0.88	0.48	-0.25
	RGL	0.22	-0.28	-0.62	-0.01	0.41	0.80	0.76	0.05	0.68	0.50	0.46
M6	ZASIA	0.63	0.04	-0.68	0.14	0.33	0.83	0.91	-0.08	n.a.	0.44	-0.47
	RGL	0.64	-0.29	-0.71	-0.22	0.21	0.86	0.88	-0.12	n.a.	0.66	0.40
M7	ZASIA	0.58	0.16	-0.80	0.22	-0.16	0.93	0.86	0.02	n.a.	0.65	-0.64
	RGL	0.67	-0.05	-0.80	0.05	0.38	0.84	0.79	-0.04	n.a.	0.55	0.34
M8	ZASIA	-0.07	0.15	-0.82	-0.05	0.22	0.93	0.87	-0.01	0.82	0.65	-0.59
	RGL	-0.24	0.10	-0.82	-0.07	0.40	0.92	0.77	-0.03	-0.77	0.39	0.16
M9	ZASIA	0.77	0.27	-0.49	0.03	-0.63	0.92	0.84	-0.05	0.66	0.45	-0.13
	RGL	0.57	-0.14	-0.61	0.10	0.00	0.90	0.78	0.22	0.06	0.20	0.35
M10	ZASIA	0.32	-0.10	0.01	0.25	-0.51	0.72	0.70	0.20	0.31	0.39	0.21
	RGL	0.22	-0.60	-0.11	0.37	0.15	0.83	0.48	0.17	0.89	0.09	0.54
M11	ZASIA	0.19	0.14	0.37	-0.13	-0.29	0.55	0.53	0.36	0.18	0.22	0.35
	RGL	0.23	-0.47	0.46	-0.01	0.04	0.65	0.13	0.59	0.53	0.24	0.65
M12	ZASIA	0.11	0.26	0.53	0.52	-0.46	0.46	0.47	0.22	0.21	0.30	0.40
	RGL	0.27	-0.52	0.67	0.33	-0.25	0.13	0.17	0.19	0.47	0.43	0.42

Figure S1 (a) Map of locations of airports in South and East Asia from the Comprehensive Observation Network for TRace gases by AIrLiner (CONTRAIL) project (Machida et al., 2008). **(b)** Close-up map for airports in Japan and Republic of Korea. The whole region is divided into four subregions, namely East Asia (EAS), the Indian sub-continent (IND), Northern Southeast Asia (NSA) and Southern Southeast Asia (SSA), and all the airports and vertical profiles are grouped into the four subregions accordingly. The zoomed grid of the LMDz-INCA model is also plotted as background.

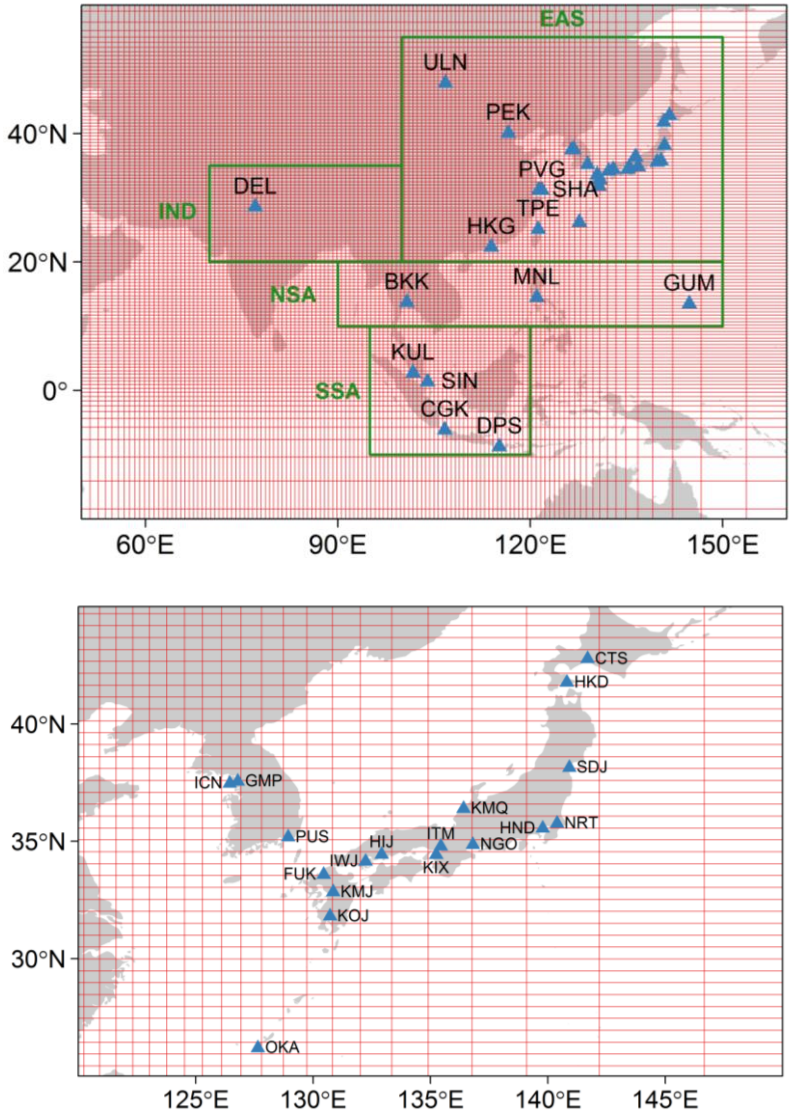

Figure S2 Sampling dates of CO_2 measurements for airports in Figure S1. For each airport, only sampling dates with vertical profiles available (i.e. measurements during ascending or descending flights) are plotted.

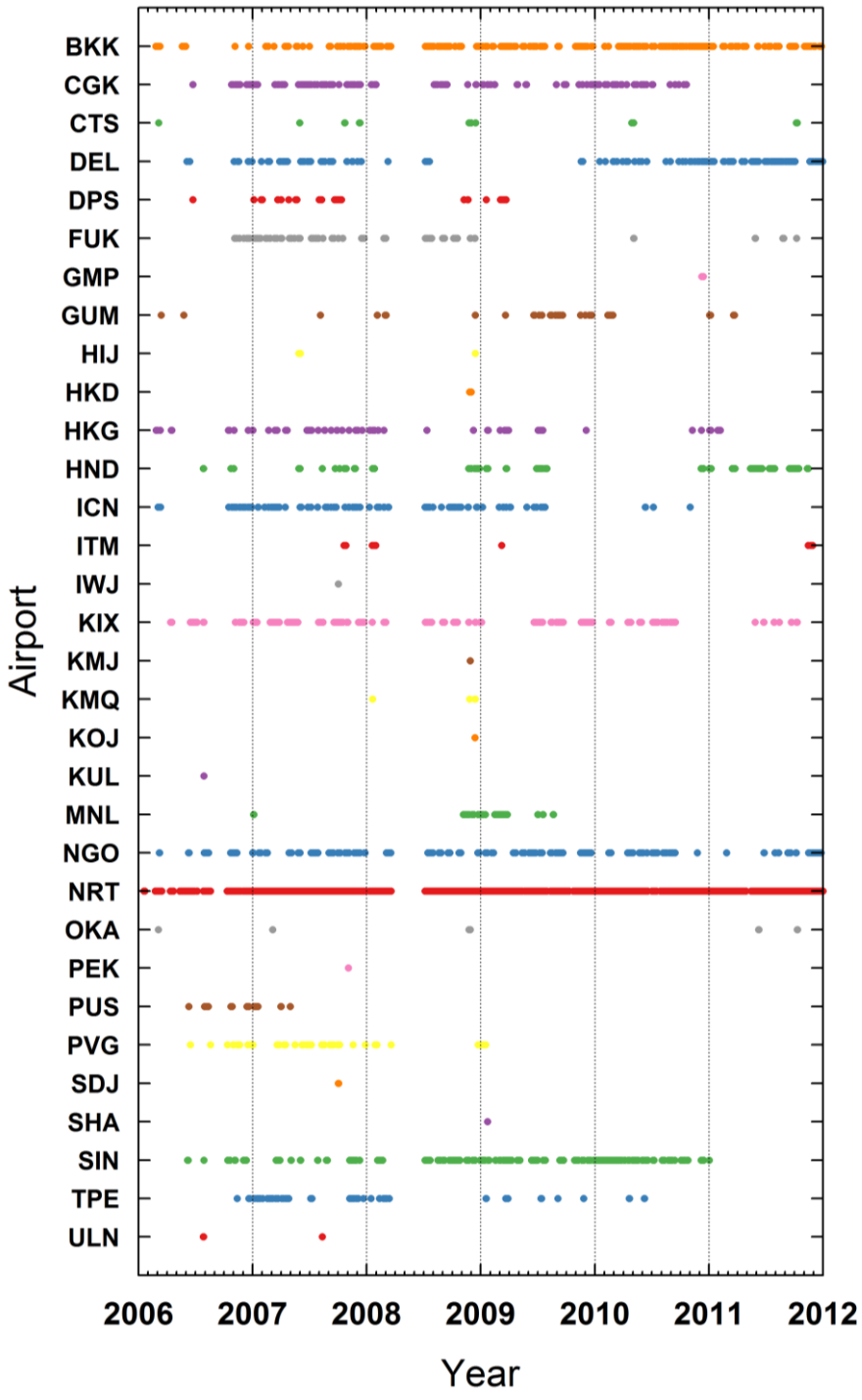

Figure S3 Scatterplots of simulated and observed CH_4 mean annual gradients between HLE and other stations for April–June (a, b), July–September (c, d), October–December (e, f), and January–March (g, h). The simulated CH_4 gradients are based on simulations from ZASIA (a, c, e, g) and REG (b, d, f, h), respectively. In each panel, the black dotted line indicates the identity line, whereas the grey solid line indicates the linear line fitted to the data. The black and grey texts give the mean bias (±1σ) and RMSE of the simulated CH_4 mean annual gradients in reference to the observed ones.

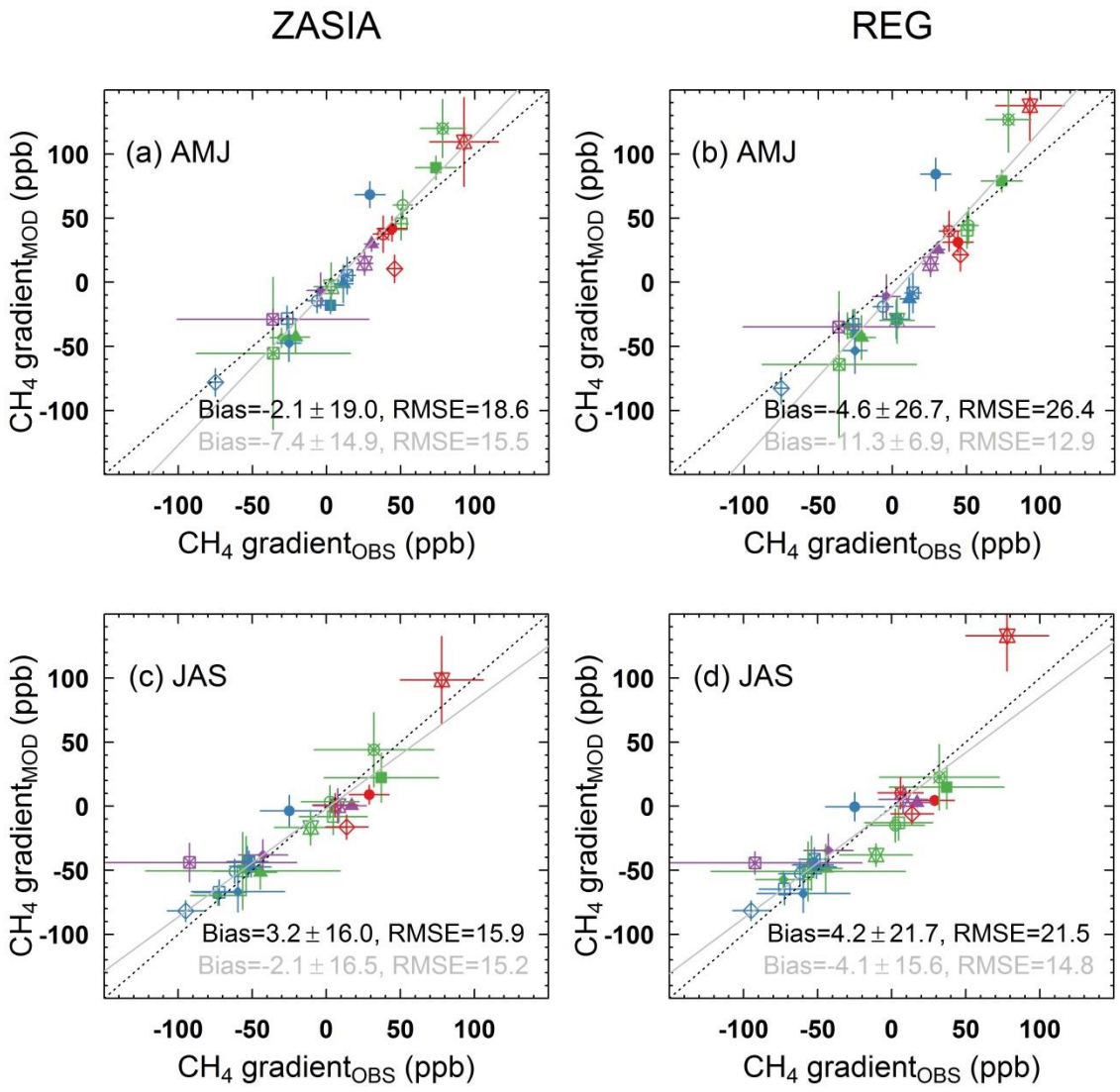

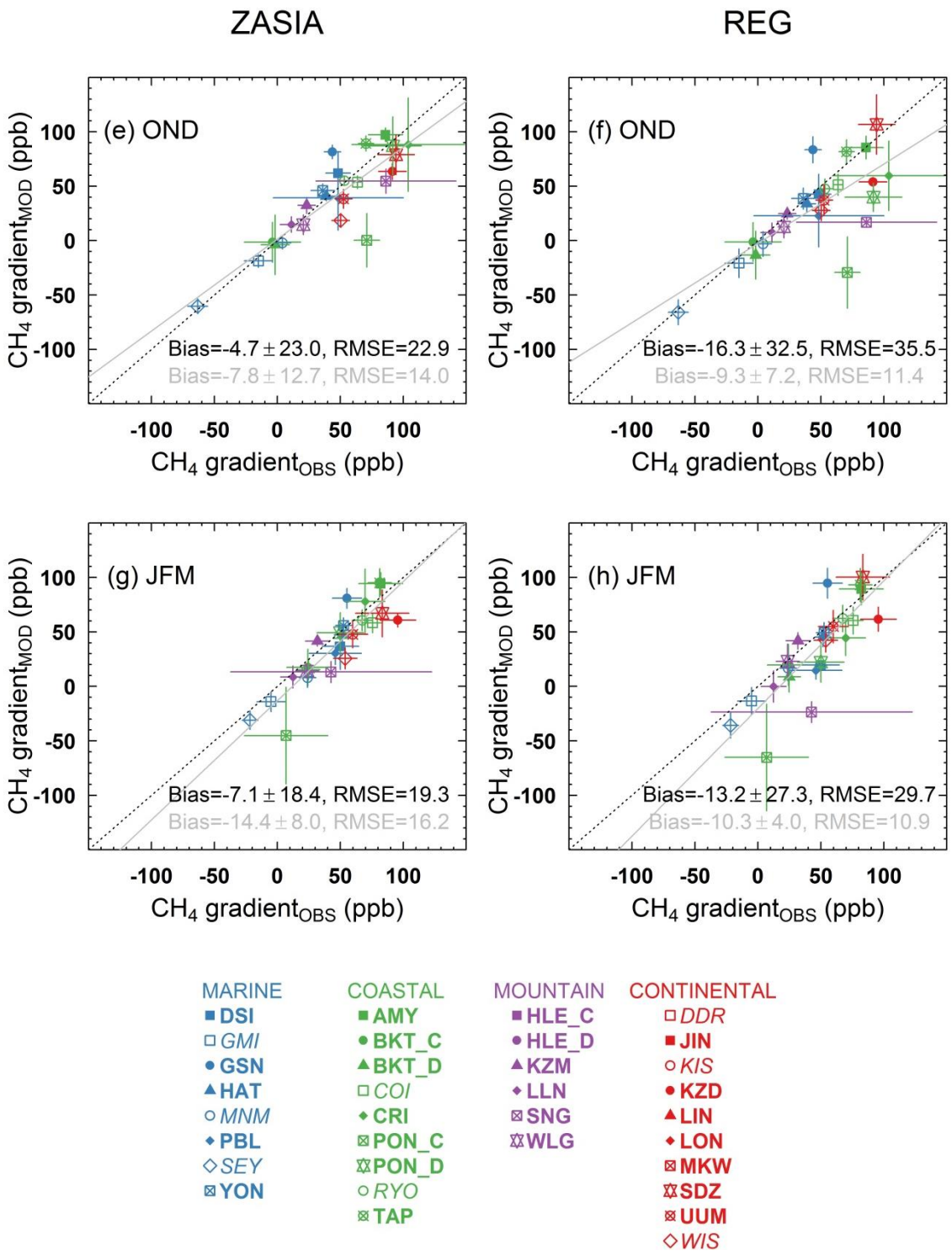
ZASIA
REG
(e) OND
(f) OND
(g) JFM
(h) JFM
CH4 gradientMOD (ppb)
CH4 gradientOBS (ppb)
Bias=-4.7 ± 23.0, RMSE=22.9
Bias=-7.8 ± 12.7, RMSE=14.0
Bias=-16.3 ± 32.5, RMSE=35.5
Bias=-9.3 ± 7.2, RMSE=11.4
Bias=-7.1 ± 18.4, RMSE=19.3
Bias=-14.4 ± 8.0, RMSE=16.2
Bias=-13.2 ± 27.3, RMSE=29.7
Bias=-10.3 ± 4.0, RMSE=10.9
MARINE
DSI
GMI
GSN
HAT
MNM
PBL
SEY
YON
COASTAL
AMY
BKT_C
BKT_D
COI
CRI
PON_C
PON_D
RYO
TAP
MOUNTAIN
HLE_C
HLE_D
KZM
LLN
SNG
WLG
CONTINENTAL
DDR
JIN
KIS
KZD
LIN
LON
MKW
SDZ
UUM
WIS

Figure S4 CH_4 surface flux maps for South and East Asia (SEA), based on two different inventories of anthropogenic emissions for the year 2008 from EDGARv4.2 and REASv2.1 (Kurokawa et al., 2013). CH_4 hotspots, defined as grids with 1% top emission rates, are indicated by blue dots. Both maps are generated in ZASIA grid meshes and with the same biogenic CH_4 fluxes as given in Table 1.

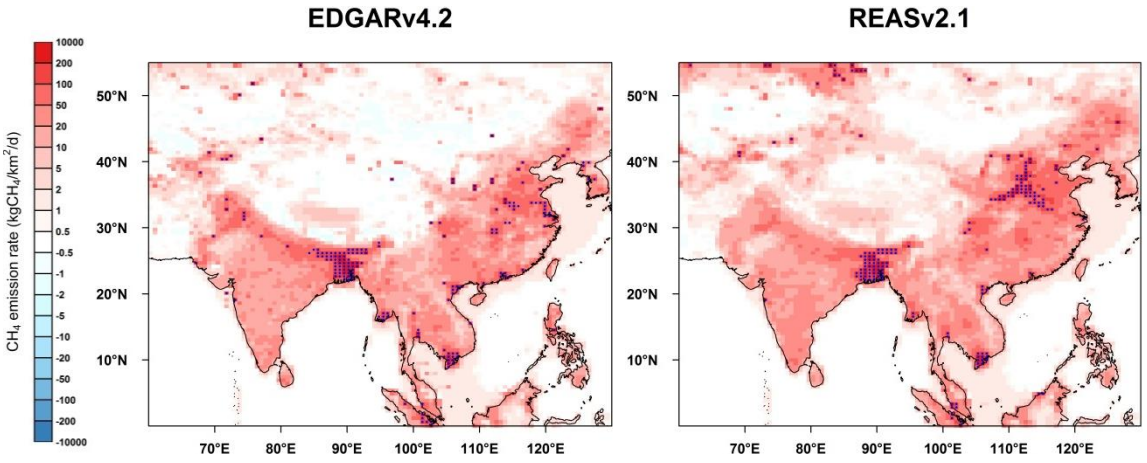

Figure S5 Maps of CH_4 surface fluxes (upper panels) and CH_4 concentration fields at the first model level (lower panels) for the year 2010. Results from both ZASIA and REG are presented for comparison.

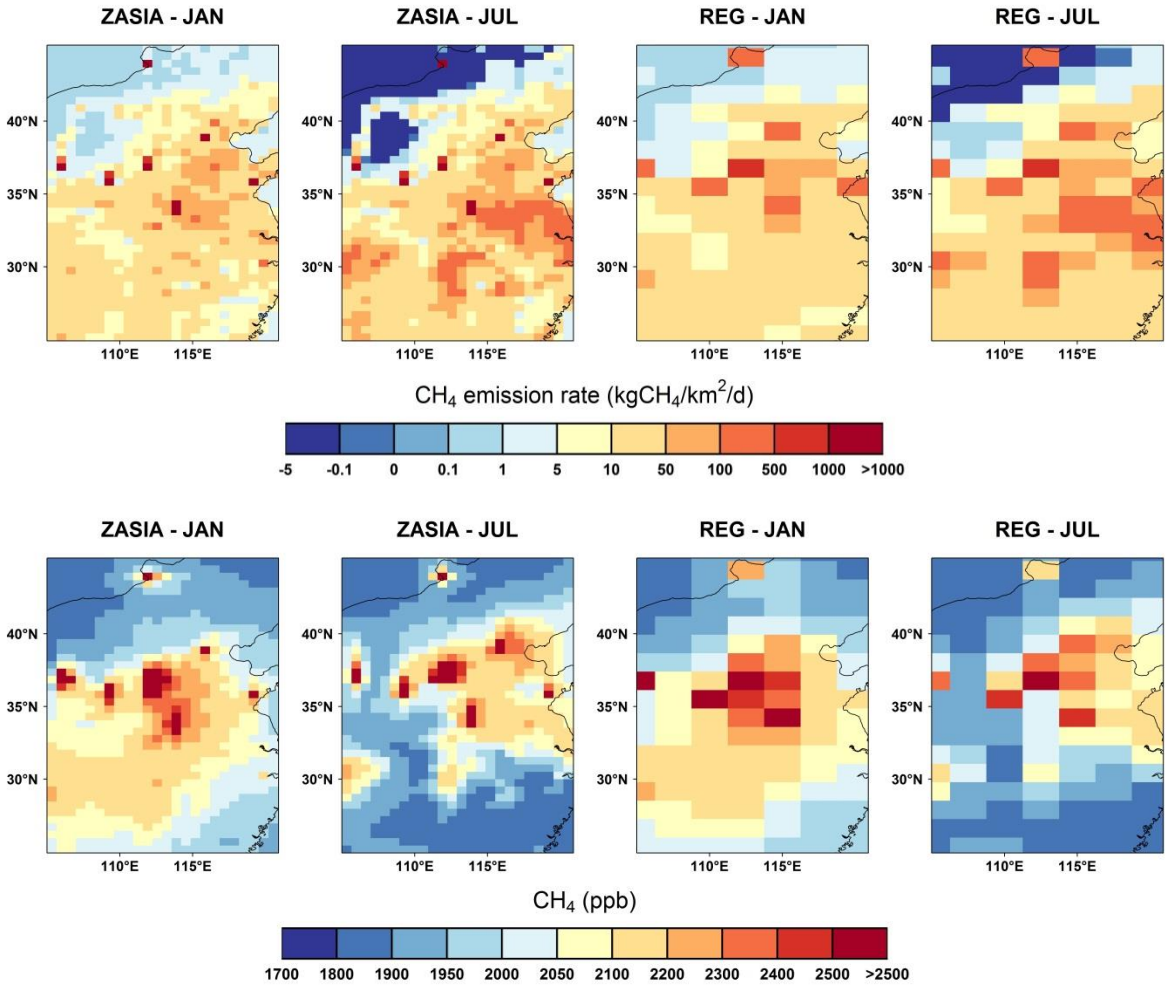

Figure S6 Model-observation comparisons on the CH_4 mean annual gradients at SDZ, PON, CRI, GSN, TAP and UUM. For each station, the left panel presents the spatial distribution of mean annual CH_4 fluxes around the station for the year 2010 mapped with the ZASIA model grids. The black meshes indicate the REG model grids. The black dot denotes the location of the station, whereas the 3×3 meshes colored in green indicate the grid where the station is located (the 'center grid') and its 8 neighbors. On the right panel, the model-observation comparison on the CH_4 mean annual gradients is shown for each of the 9 grids. The grey shades indicate the observed CH_4 mean annual gradient and its uncertainty (±1σ). The CH_4 mean annual gradients simulated from ZASIA (denoted by red dots) are plotted for each grid of the 3×3 meshes from Layer 1 to Layer 7, with corresponding average layer altitudes labeled on the vertical axes. For comparison, the simulated CH_4 mean annual gradients from REG are also plotted (denoted by black dots) for the 'center grid' of the REG model grids.

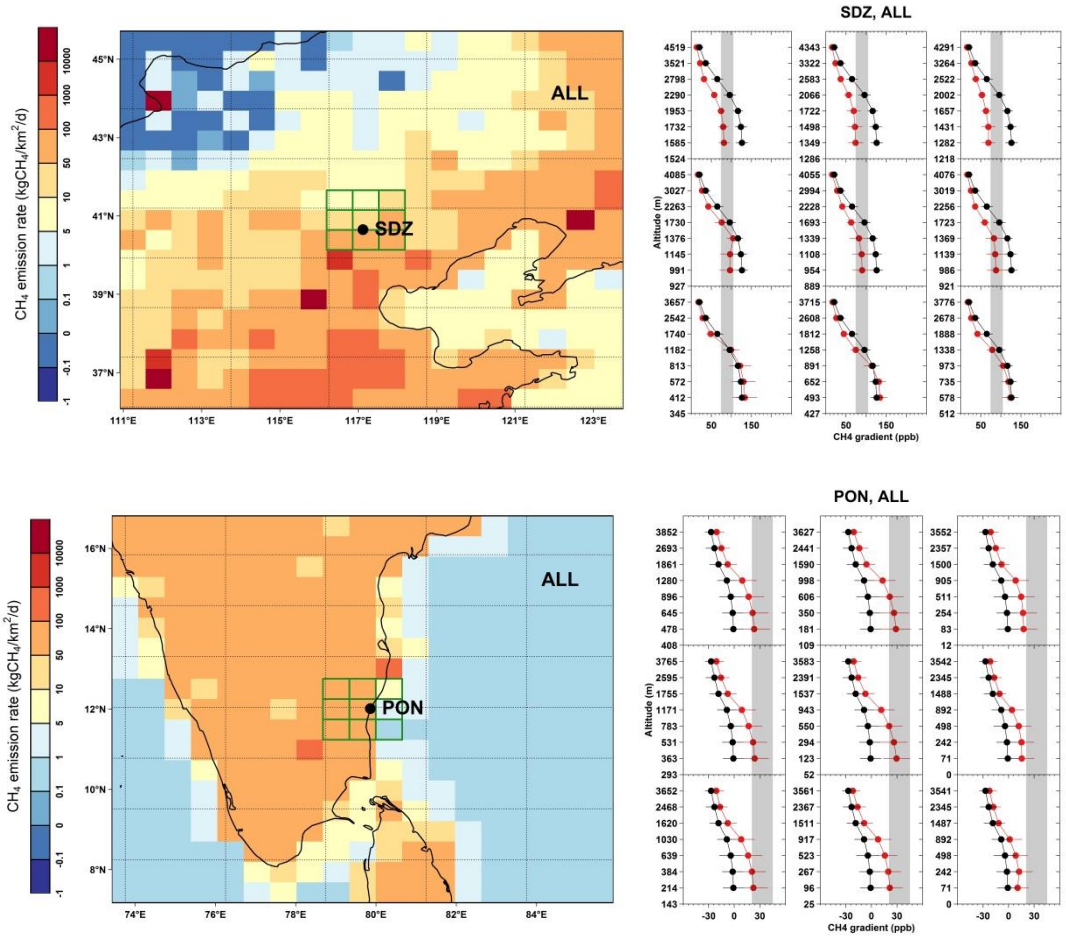

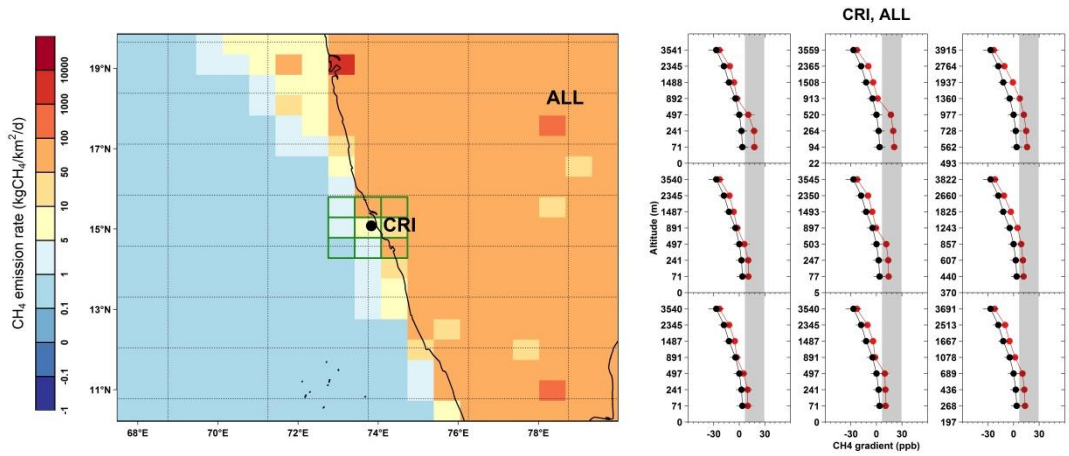
CRI, ALL
ALL
CRI
CH4 emission rate (kgCH4/km2/d)
Altitude (m)
CH4 gradient (ppb)

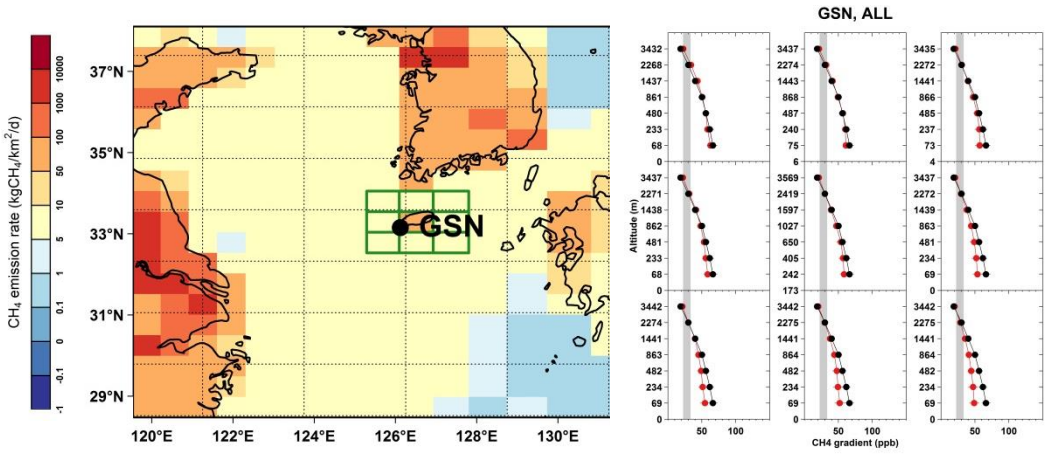
GSN, ALL
GSN
CH4 emission rate (kgCH4/km2/d)
Altitude (m)
CH4 gradient (ppb)

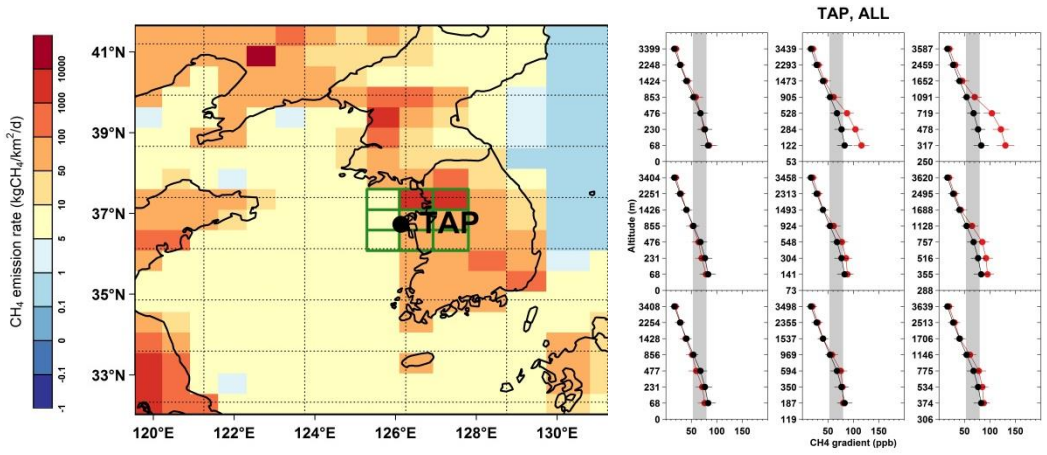
TAP, ALL
TAP
CH4 emission rate (kgCH4/km2/d)
Altitude (m)
CH4 gradient (ppb)

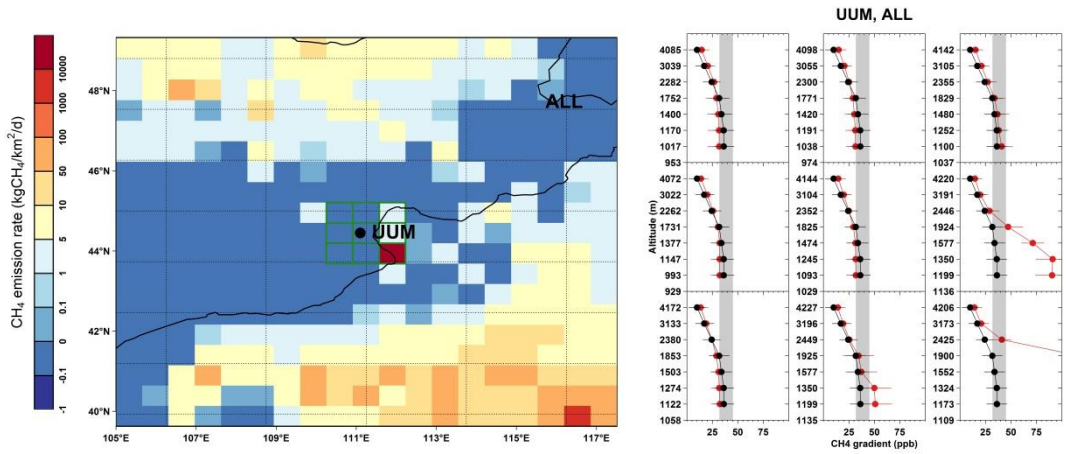
CH4 emission rate (kgCH4/km2/d)
-1
-0.1
0
0.1
1
5
10
50
100
1000
10000
48°N
46°N
44°N
42°N
40°N
105°E
107°E
109°E
111°E
113°E
115°E
117°E
ALL
UUM
UUM, ALL
Altitude (m)
CH4 gradient (ppb)
25
50
75

Figure S7 Scatterplots of simulated and observed CO_2 mean annual gradients between HLE and other stations for April–June (a, b), July–September (c, d), October–December (e, f), and January–March (g, h). The simulated CO_2 gradients are based on simulations from ZASIA (a, c, e, g) and REG (b, d, f, h), respectively. In each panel, the black dotted line indicates the identity line, whereas the grey solid line indicates the linear line fitted to the data. The black and grey texts give the mean bias (±1σ) and RMSE of the simulated CO_2 mean annual gradients in reference to the observed ones.

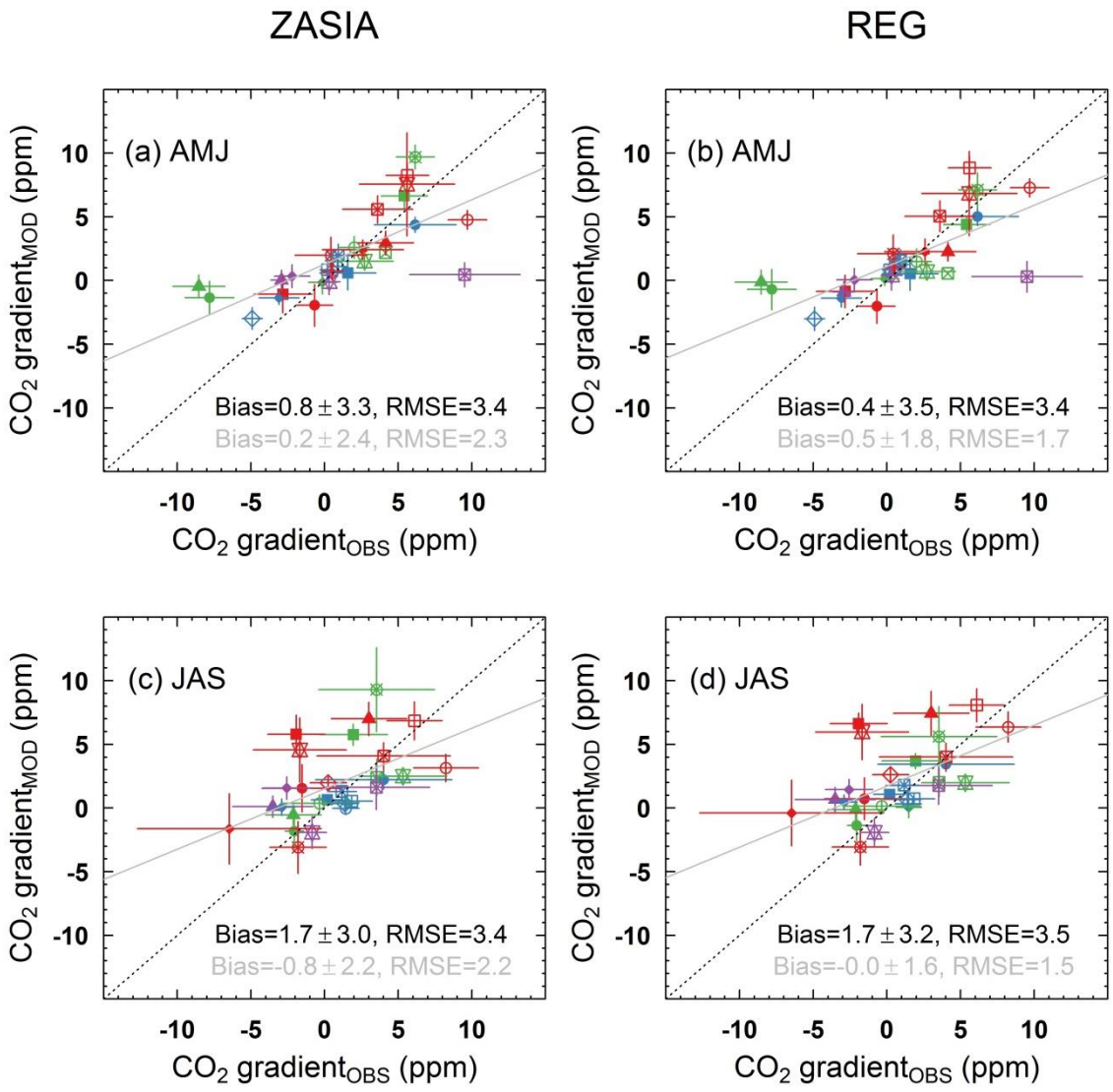

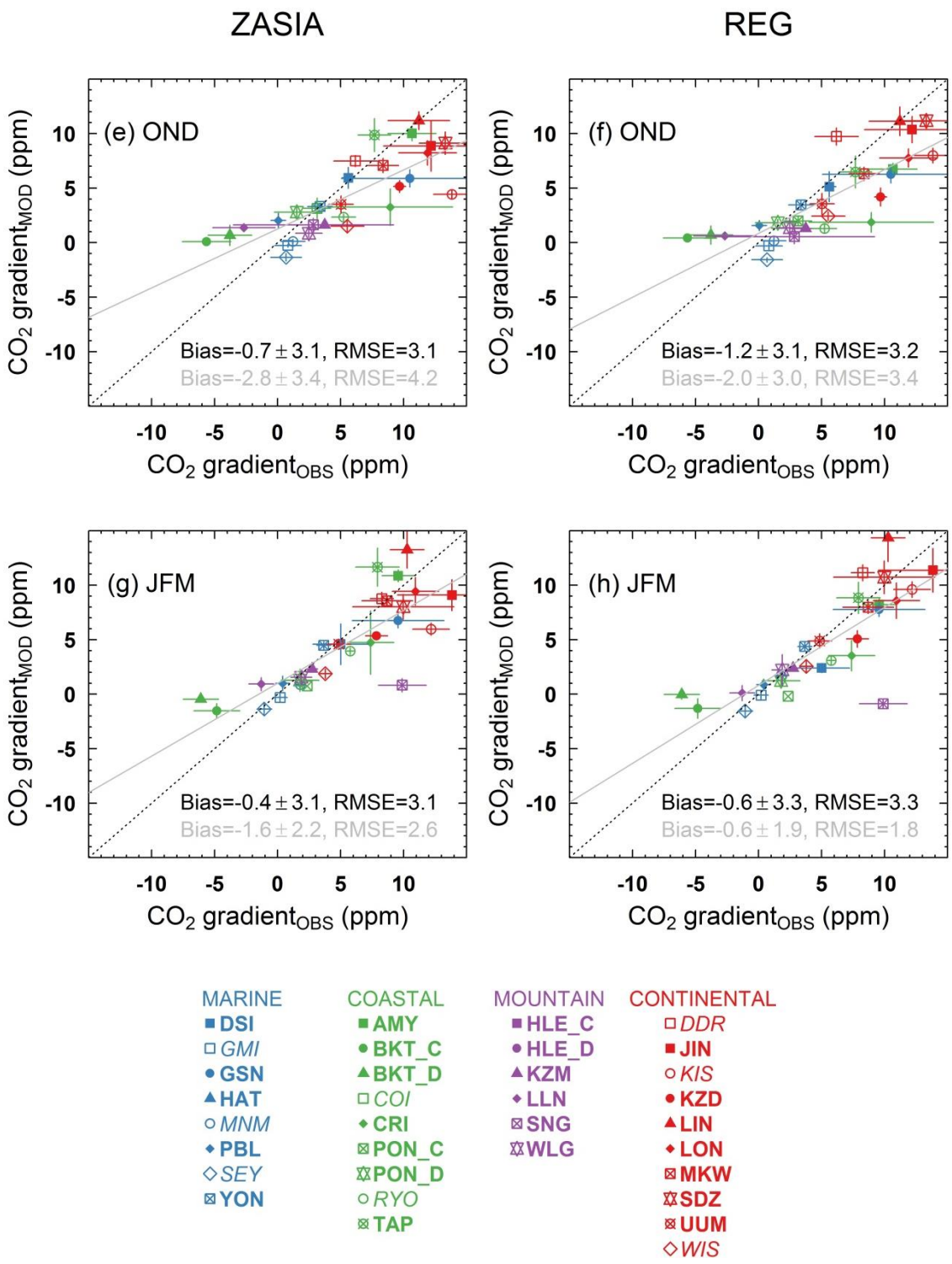
ZASIA
REG
(e) OND
(f) OND
(g) JFM
(h) JFM
CO2 gradientMOD (ppm)
CO2 gradientOBS (ppm)
Bias=-0.7±3.1, RMSE=3.1
Bias=-2.8±3.4, RMSE=4.2
Bias=-1.2±3.1, RMSE=3.2
Bias=-2.0±3.0, RMSE=3.4
Bias=-0.4±3.1, RMSE=3.1
Bias=-1.6±2.2, RMSE=2.6
Bias=-0.6±3.3, RMSE=3.3
Bias=-0.6±1.9, RMSE=1.8
MARINE
DSI
GMI
GSN
HAT
MNM
PBL
SEY
YON
COASTAL
AMY
BKT_C
BKT_D
COI
CRI
PON_C
PON_D
RYO
TAP
MOUNTAIN
HLE_C
HLE_D
KZM
LLN
SNG
WLG
CONTINENTAL
DDR
JIN
KIS
KZD
LIN
LON
MKW
SDZ
UUM
WIS

Figure S8 Model-observation comparisons on the CO_2 mean annual gradients at TAP. The left panel presents the spatial distribution of mean annual CO_2 fluxes around the station for the year 2010 mapped with the ZASIA model grids. The black meshes indicate the REG model grids. The black dot denotes the location of the station, whereas the 3×3 meshes colored in green indicate the grid where the station is located (the 'center grid') and its 8 neighbors. On the right panel, the model-observation comparison on the CO_2 mean annual gradients is shown for each of the 9 grids. The grey shades indicate the observed CO_2 mean annual gradient and its uncertainty (±1σ). The CO_2 mean annual gradients simulated from ZASIA (denoted by red dots) are plotted for each grid of the 3×3 meshes from Layer 1 to Layer 7, with corresponding average layer altitudes labeled on the vertical axes. For comparison, the simulated CO_2 mean annual gradients from REG are also plotted (denoted by black dots) for the 'center grid' of the REG model grids.

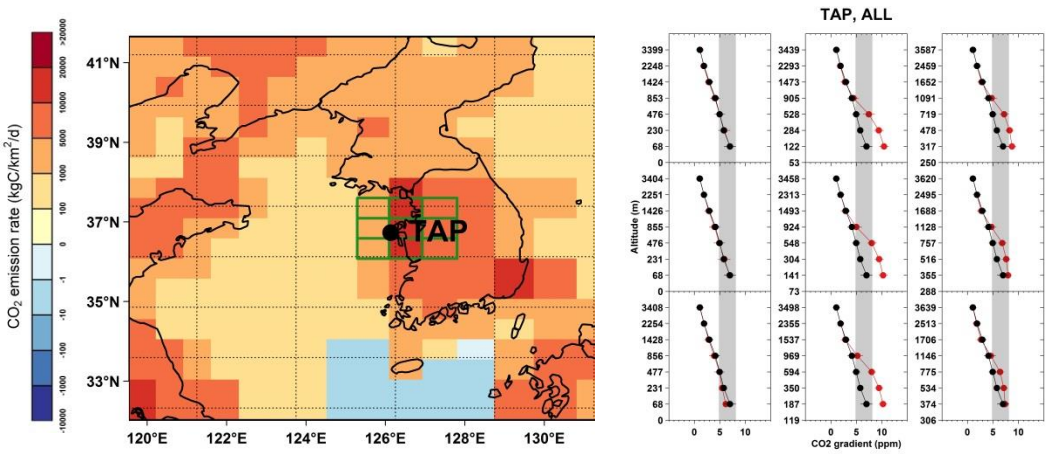

Figure S9 Model-observation comparisons on the CH_4 seasonal cycles at HLE, WLG, KZM, SDZ, TAP, GSN, BKT, SNG and CRI. For each station, the left panel presents the spatial distribution of mean annual CH_4 fluxes around the station for the year 2010 mapped with the ZASIA model grids. The black meshes indicate the REG model grids. The black dot denotes the location of the station, whereas the 3×3 meshes colored in green indicate the grid where the station is located (the 'center grid') and its 8 neighbors. On the right panel, the model-observation comparison on the CH_4 mean seasonal cycles is shown for each of the 9 grids. The grey shades indicate the observed CH_4 mean seasonal cycle and its uncertainty (±1σ) calculated from 1000 bootstrap replicates. The CH_4 mean seasonal cycles simulated from ZASIA (denoted by colored solid lines) are plotted for each grid of the 3×3 meshes and for different layers. For comparison, the simulated CH_4 mean seasonal cycles from REG are also plotted (denoted by colored dotted lines) for the 'center grid' of the REG model grids.

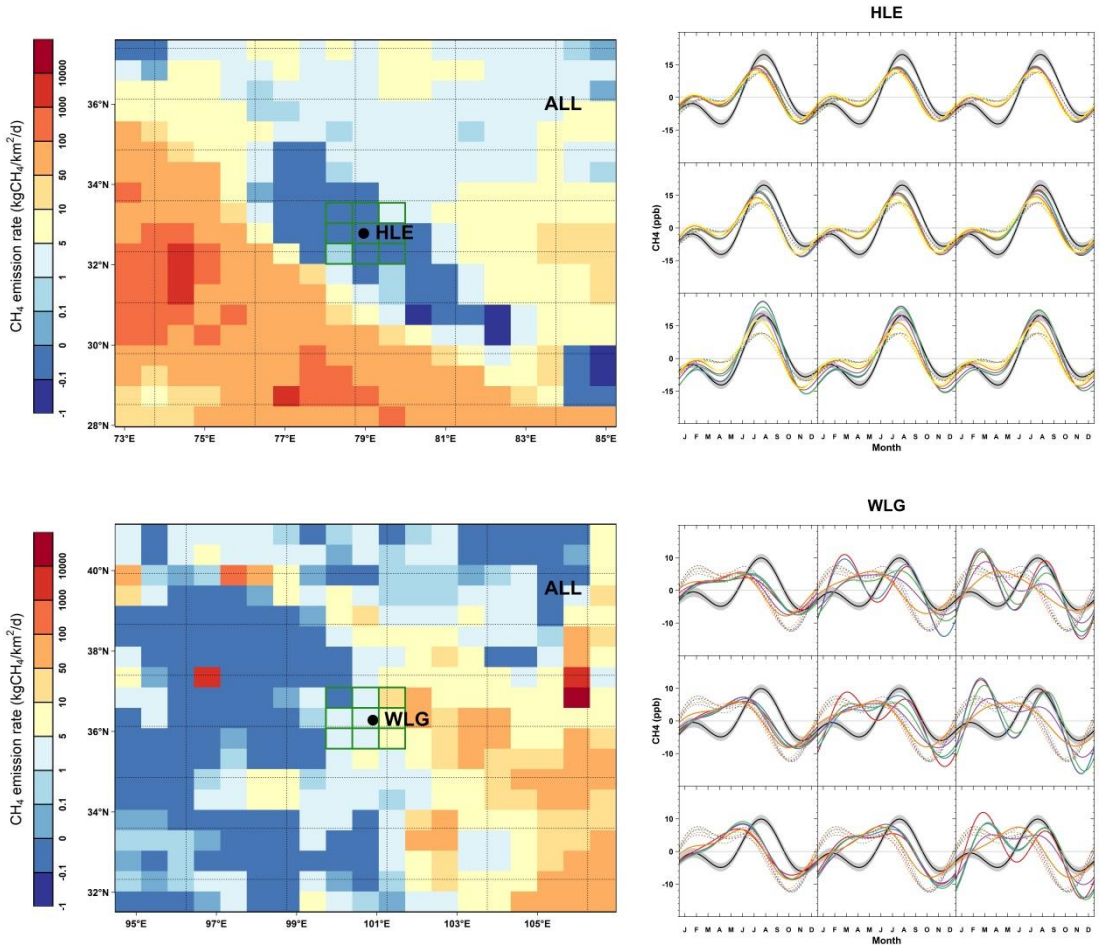

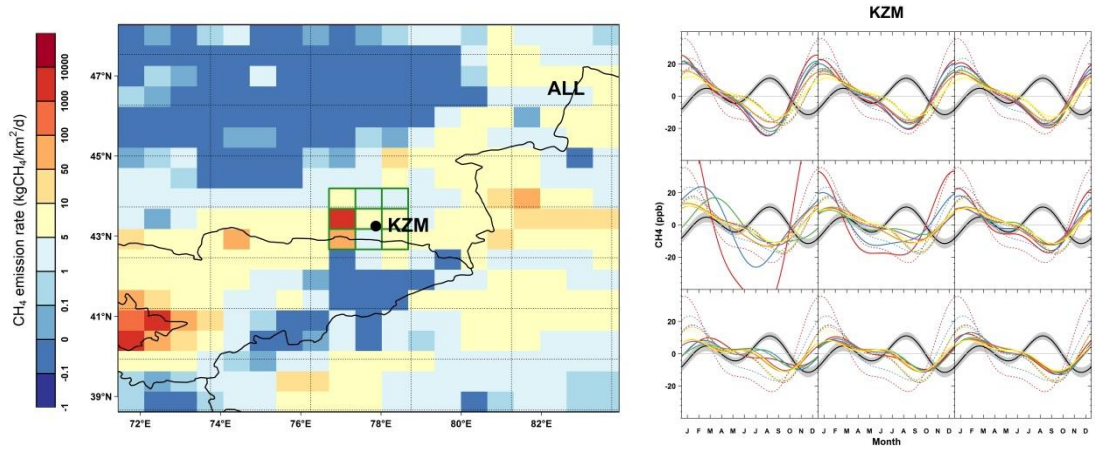
KZM
ALL
KZM
CH4 emission rate (kgCH4/km2/d)
CH4 (ppb)
Month

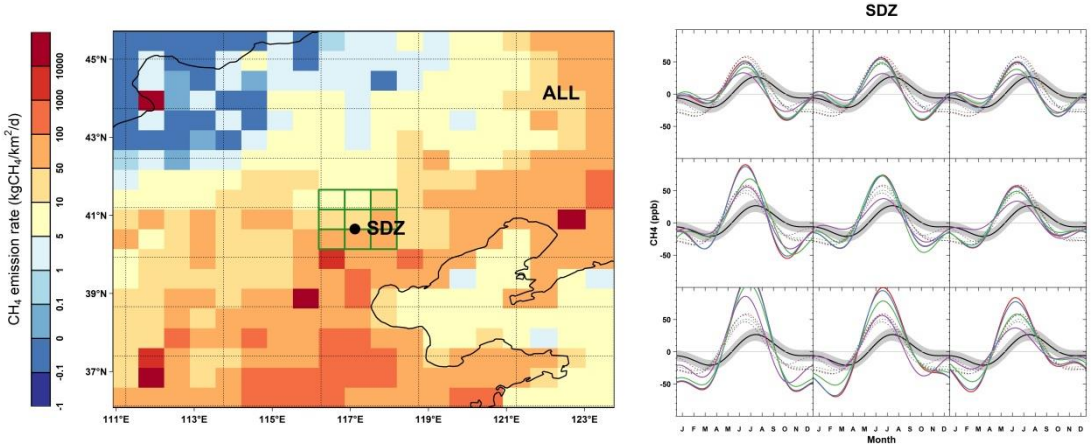
SDZ
ALL
SDZ
CH4 emission rate (kgCH4/km2/d)
CH4 (ppb)
Month

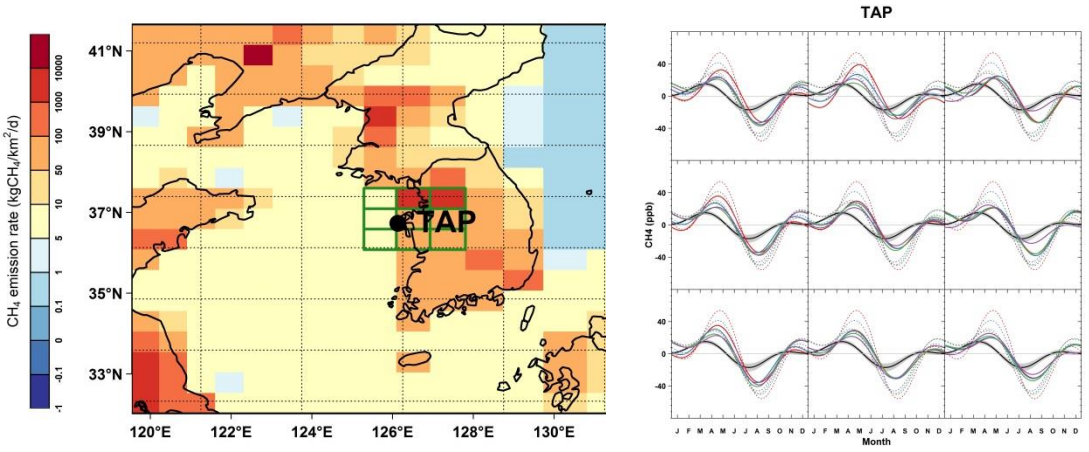
TAP
TAP
CH4 emission rate (kgCH4/km2/d)
CH4 (ppb)
Month

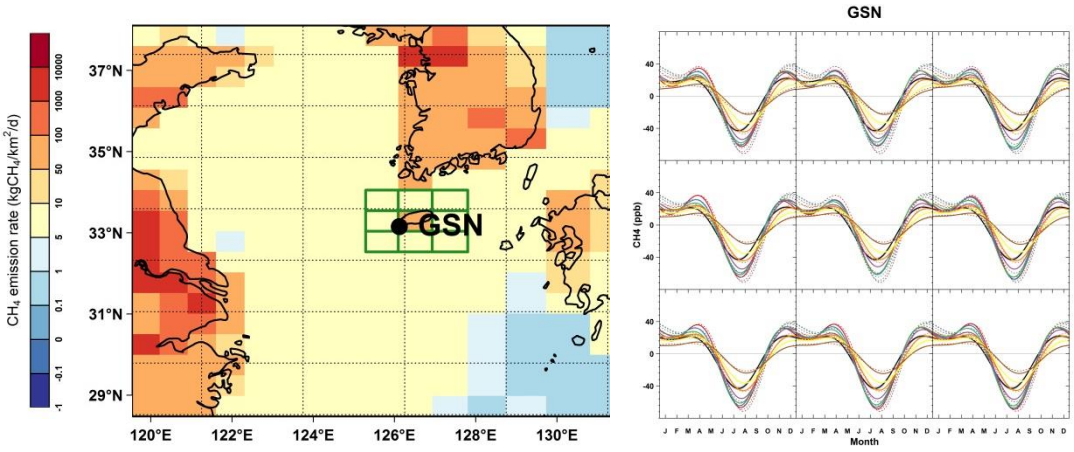
GSN
CH_4 emission rate ($kgCH_4/km^2/d$)
-1
-0.1
0
0.1
1
5
10
50
100
1000
10000
37°N
35°N
33°N
31°N
29°N
120°E
122°E
124°E
126°E
128°E
130°E
GSN
CH4 (ppb)
40
0
-40
J F M A M J J A S O N D J F M A M J J A S O N D J F M A M J J A S O N D
Month

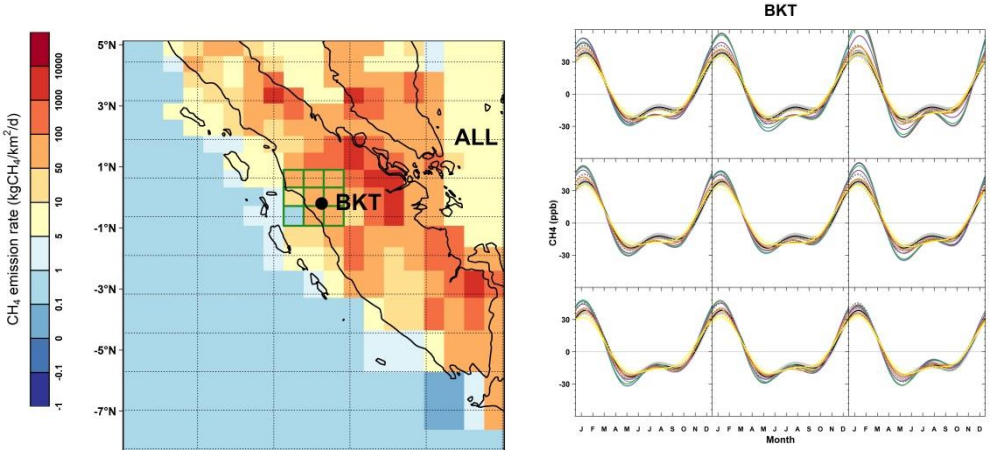
BKT
CH_4 emission rate ($kgCH_4/km^2/d$)
-1
-0.1
0
0.1
1
5
10
50
100
1000
10000
5°N
3°N
1°N
-1°N
-3°N
-5°N
-7°N
ALL
BKT
CH4 (ppb)
30
0
-30
J F M A M J J A S O N D J F M A M J J A S O N D J F M A M J J A S O N D
Month

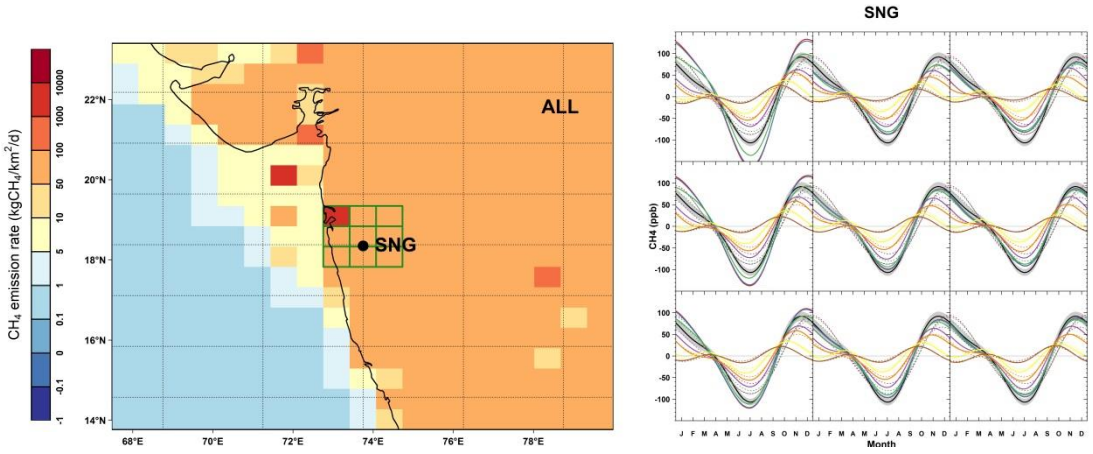
SNG
CH_4 emission rate ($kgCH_4/km^2/d$)
-1
-0.1
0
0.1
1
5
10
50
100
1000
10000
22°N
20°N
18°N
16°N
14°N
68°E
70°E
72°E
74°E
76°E
78°E
ALL
SNG
CH4 (ppb)
100
50
0
-50
-100
J F M A M J J A S O N D J F M A M J J A S O N D J F M A M J J A S O N D
Month

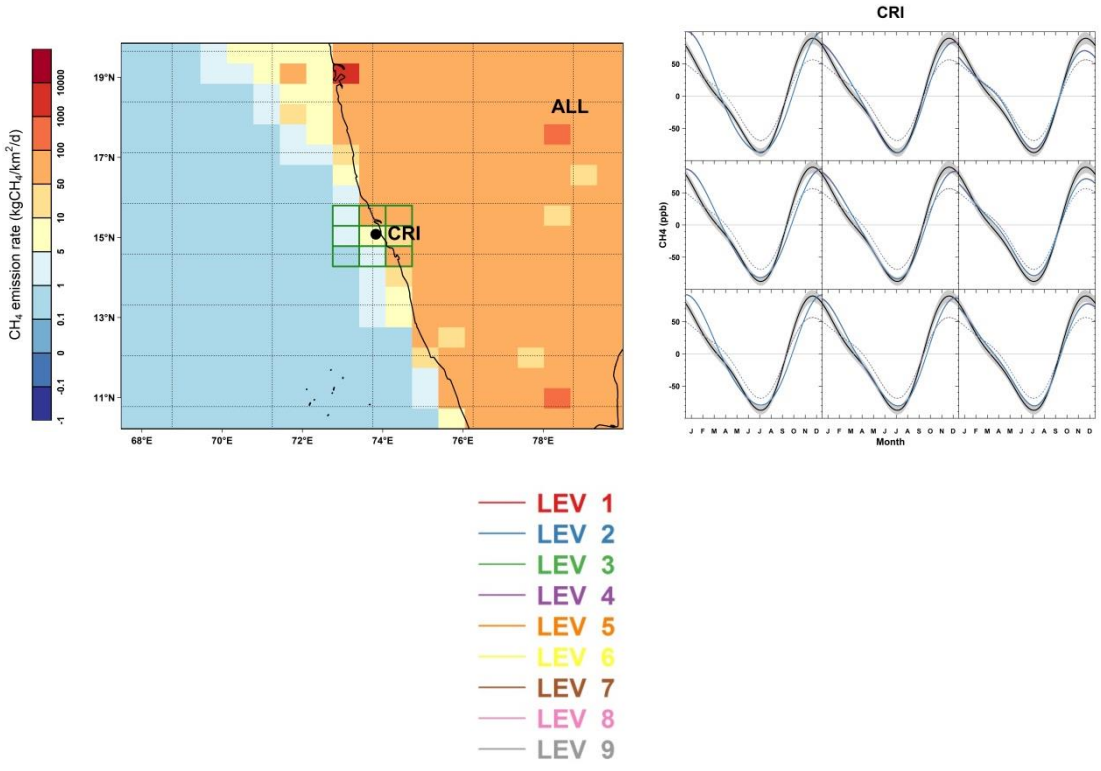
CH4 emission rate (kgCH4/km2/d)
-1
-0.1
0
0.1
1
5
10
50
100
1000
10000
19°N
17°N
15°N
13°N
11°N
68°E
70°E
72°E
74°E
76°E
78°E
ALL
CRI
CRI
CH4 (ppb)
50
0
-50
J F M A M J J A S O N D J F M A M J J A S O N D J F M A M J J A S O N D
Month
LEV 1
LEV 2
LEV 3
LEV 4
LEV 5
LEV 6
LEV 7
LEV 8
LEV 9

Figure S10 Model-observation comparisons on the CO_2 seasonal cycles at HLE, SNG, CRI, GSN and KIS. For each station, the left panel presents the spatial distribution of mean annual CO_2 fluxes around the station for the year 2010 mapped with the ZASIA model grids. The black meshes indicate the REG model grids. The black dot denotes the location of the station, whereas the 3×3 meshes colored in green indicate the grid where the station is located (the 'center grid') and its 8 neighbors. On the right panel, the model-observation comparison on the CO_2 mean seasonal cycles is shown for each of the 9 grids. The grey shades indicate the observed CO_2 mean seasonal cycle and its uncertainty (±1σ) calculated from 1000 bootstrap replicates. The CO_2 mean seasonal cycles simulated from ZASIA (denoted by colored solid lines) are plotted for each grid of the 3×3 meshes and for different layers. For comparison, the simulated CO_2 mean seasonal cycles from REG are also plotted (denoted by colored dotted lines) for the 'center grid' of the REG model grids.

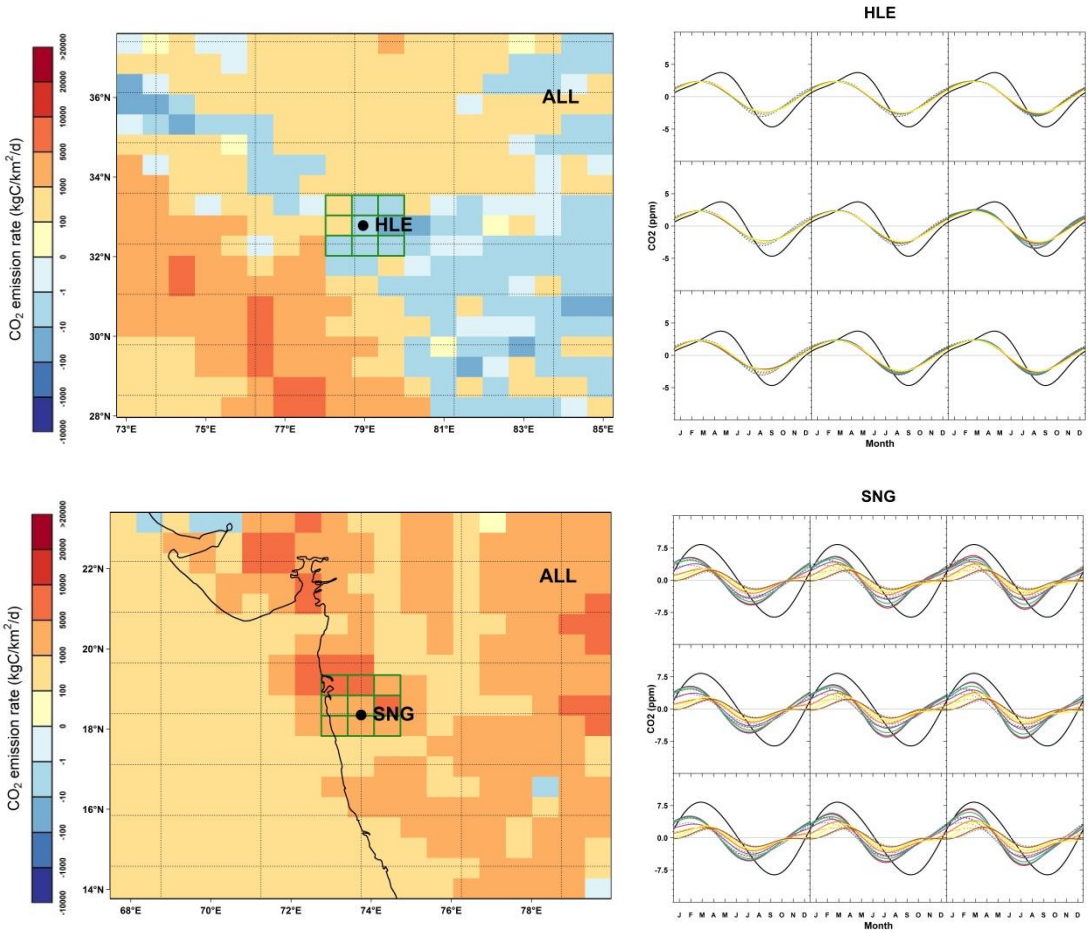

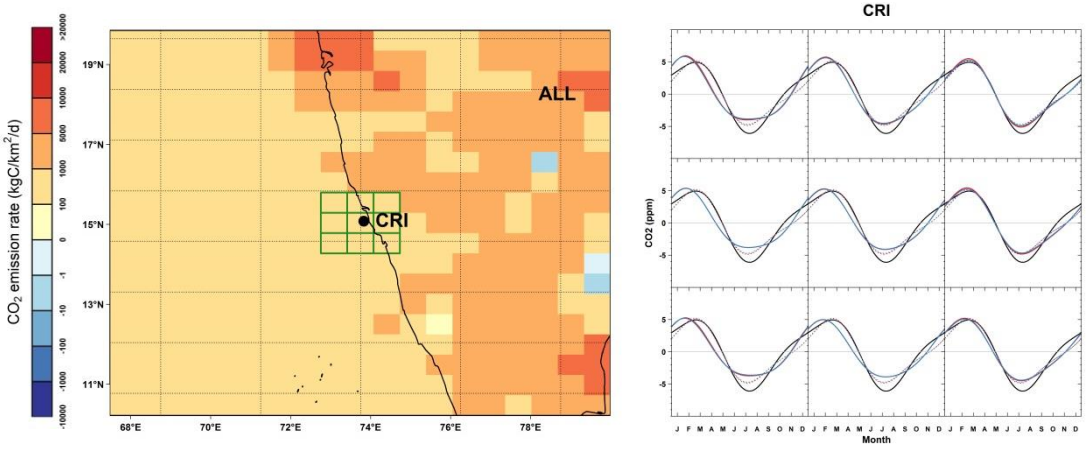

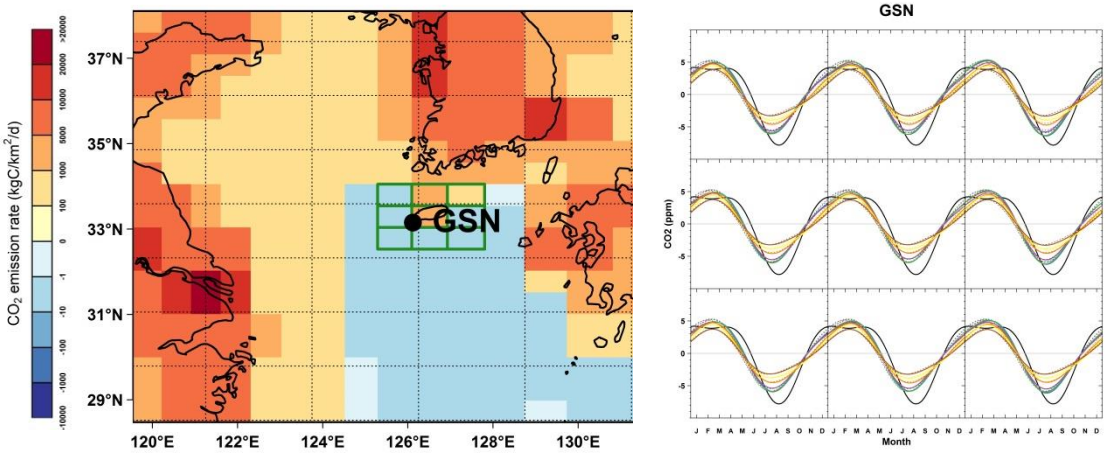

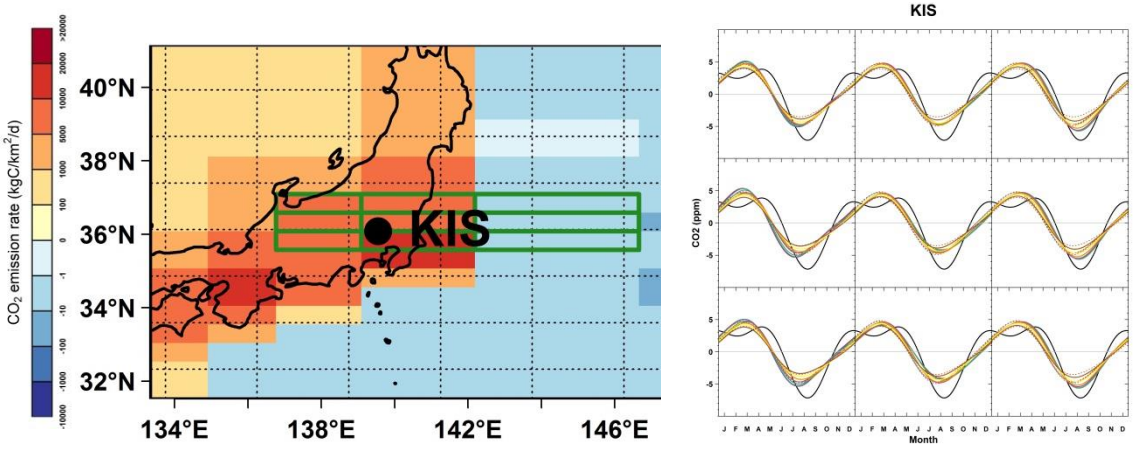

LEV 1
LEV 2
LEV 3
LEV 4
LEV 5
LEV 6
LEV 7
LEV 8
LEV 9

Figure S11 Taylor diagrams showing correlations and normalized standard deviations (NSD; the ratio of the simulated to observed standard deviation) between the simulated and observed CH_4 synoptic variability for (a,b) April–June (AMJ), (c,d) July–September (JAS), (e,f) October–December (OND) and (g,h) January–March (JFM). Results from both ZASIA (a,c,e,g) and REG (b,d,f,h) are presented. For each station, the CH_4 synoptic variability is calculated from residuals from the smoothed fitting curve.

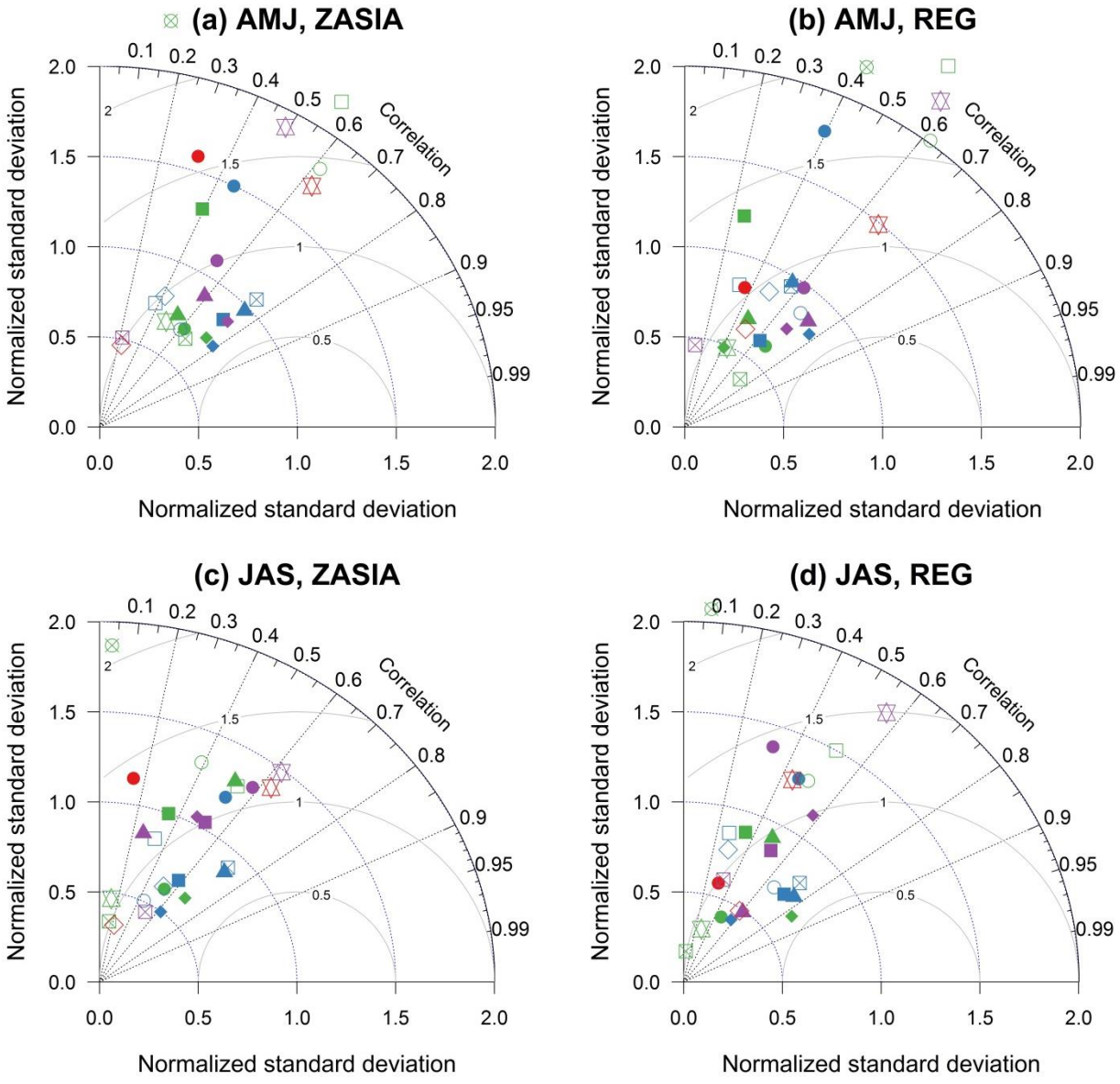

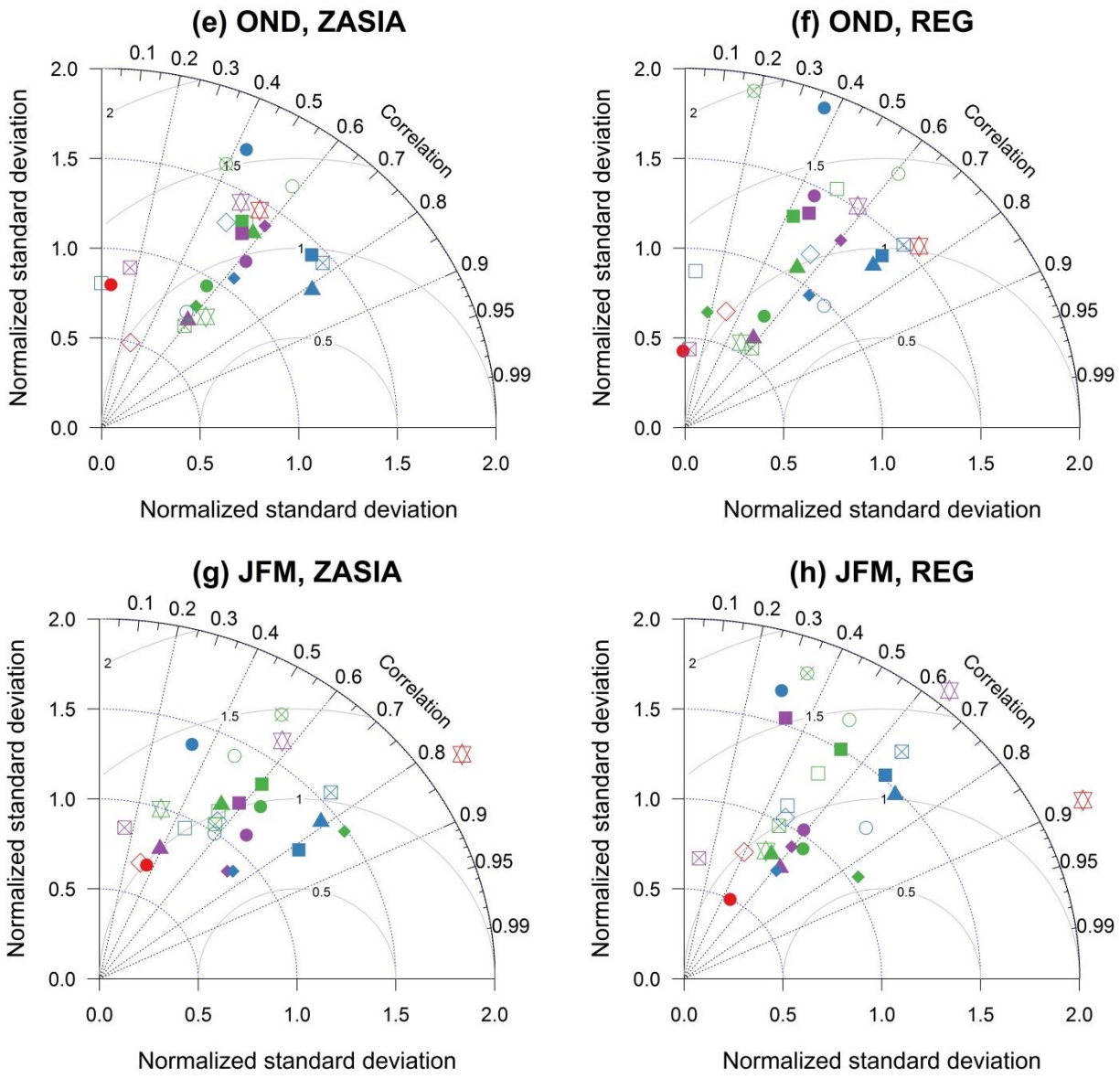

MARINE	COASTAL	MOUNTAIN	CONTINENTAL
■ **DSI**	■ **AMY**	■ **HLE_C**	□ *DDR*
□ *GMI*	● **BKT_C**	● **HLE_D**	■ **JIN**
● **GSN**	▲ **BKT_D**	▲ **KZM**	○ *KIS*
▲ **HAT**	□ *COI*	◆ **LLN**	● **KZD**
○ *MNM*	◆ **CRI**	⊠ **SNG**	▲ **LIN**
◆ **PBL**	⊠ **PON_C**	✡ **WLG**	◆ **LON**
◇ *SEY*	✡ **PON_D**		⊠ **MKW**
⊠ **YON**	○ *RYO*		✡ **SDZ**
	⊠ **TAP**		⊠ **UUM**
			◇ *WIS*

Figure S12 The CH_4 synoptic variability at CRI, SNG and SDZ simulated from ZASIA (red dots) and REG (blue dots), in comparison with the observed CH_4 synoptic variability (black dots). For each station, synoptic variability is calculated as residuals from the smoothed fitting curve. The open circles indicate the synoptic events that are not realistically simulated by ZASIA, with a model-observation deviation (absolute value) beyond four times the average.

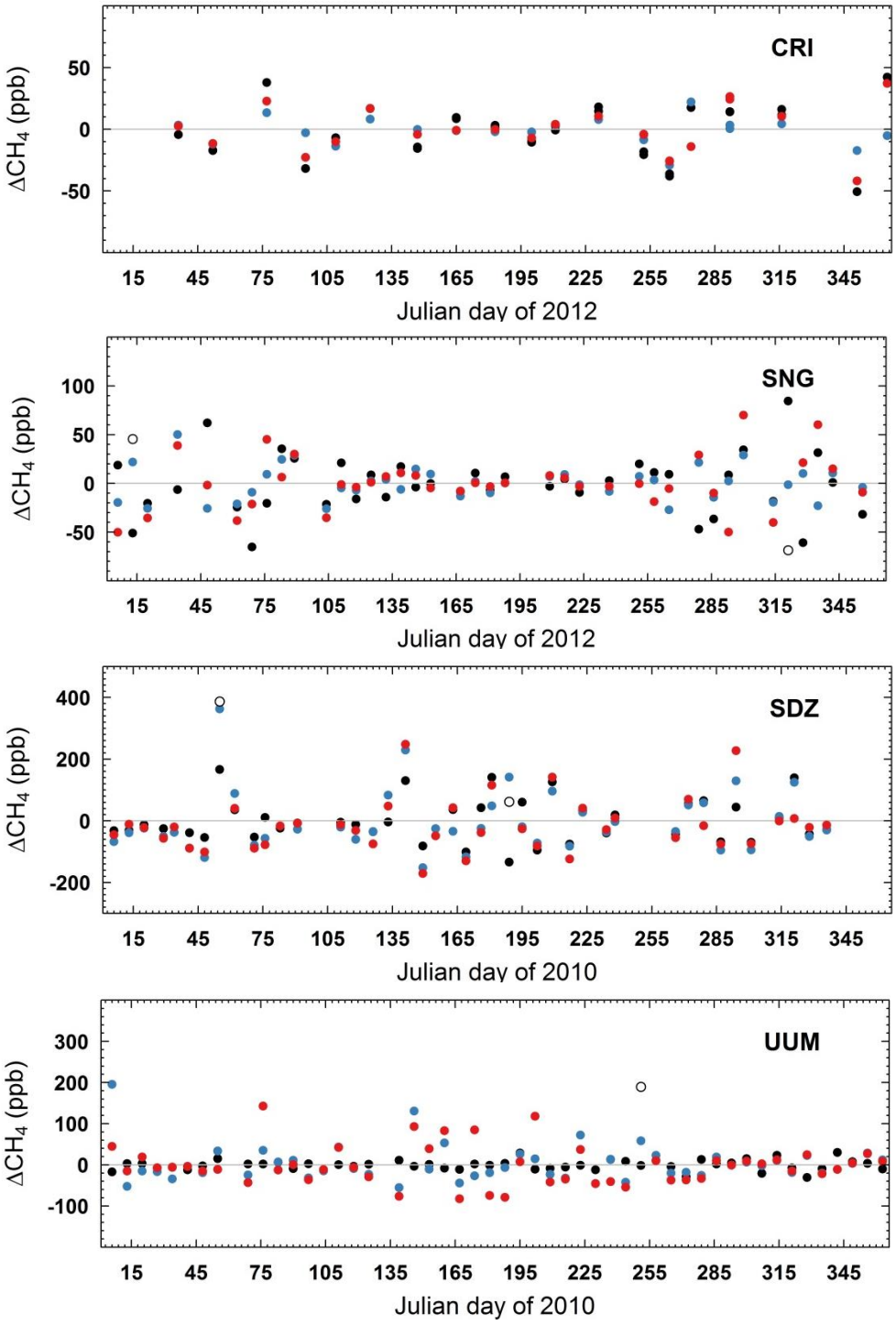

Figure S13 Taylor diagrams showing correlations and normalized standard deviations (NSD; the ratio of the simulated to observed standard deviation) between the simulated and observed CO_2 synoptic variability for (a,b) April–June (AMJ), (c,d) July–September (JAS), (e,f) October–December (OND) and (g,h) January–March (JFM). Results from both ZASIA (a,c,e,g) and REG (b,d,f,h) are presented. For each station, the CO_2 synoptic variability is calculated from residuals from the smoothed fitting curve.

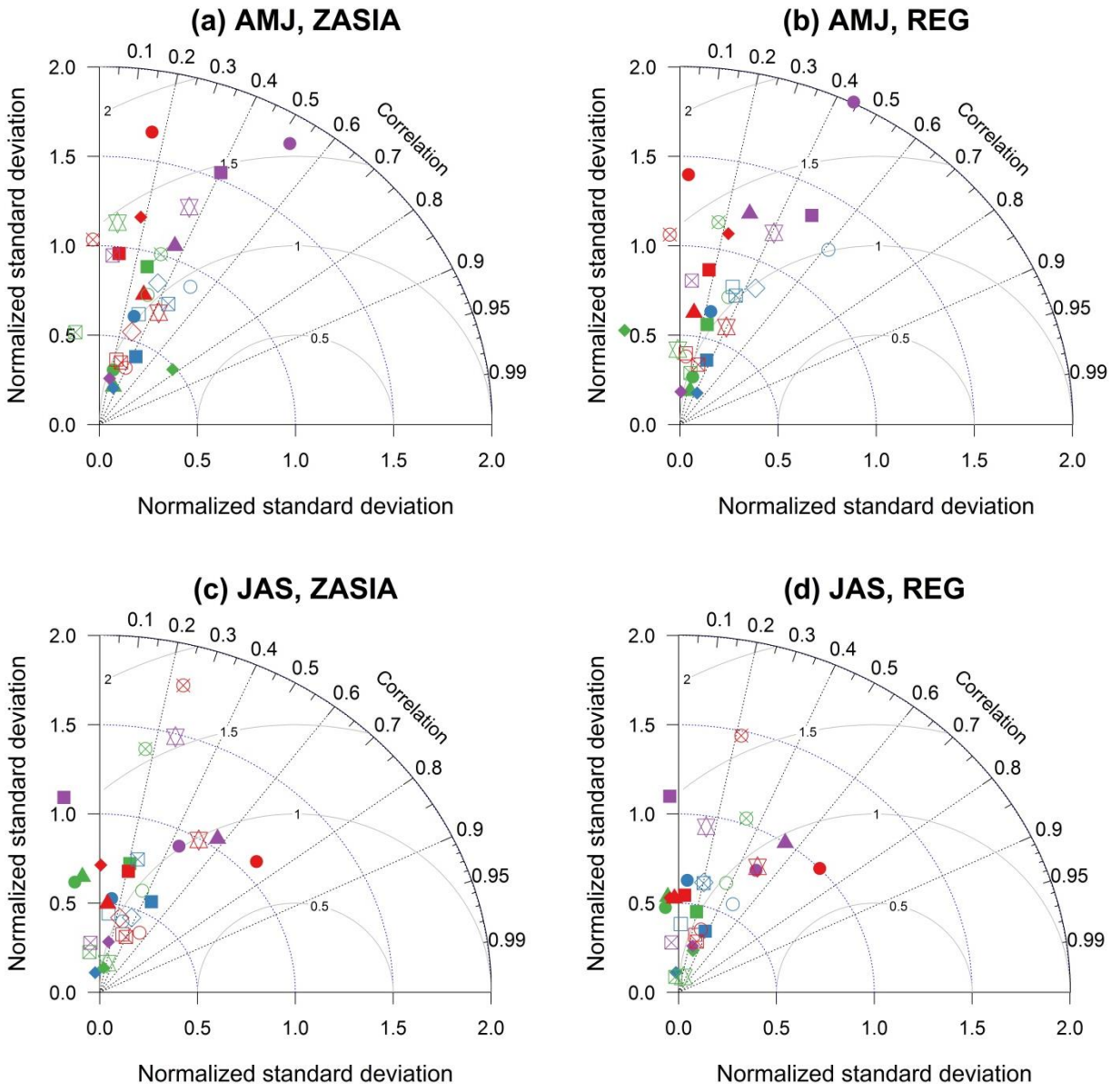

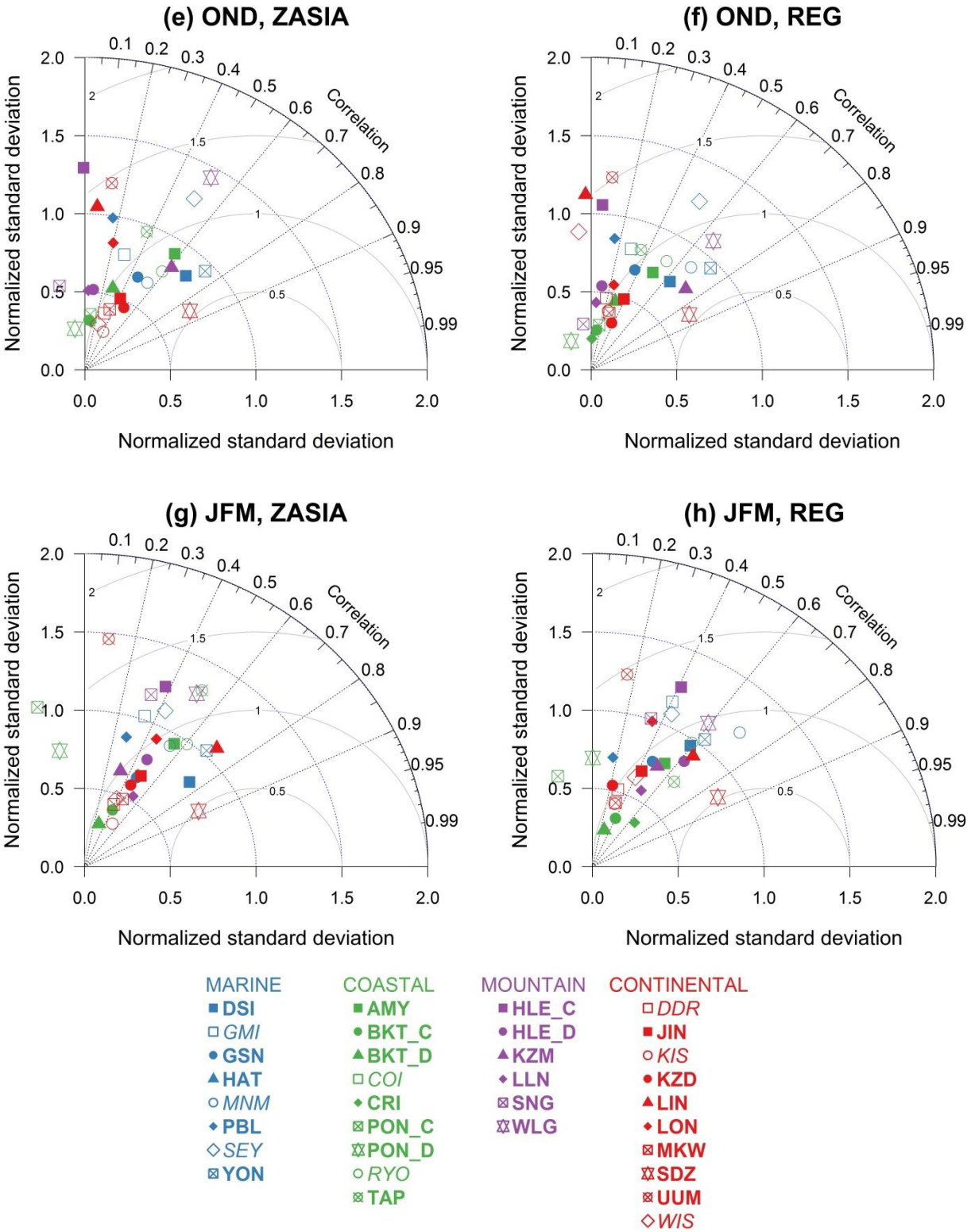
(e) OND, ZASIA
(f) OND, REG
(g) JFM, ZASIA
(h) JFM, REG
Normalized standard deviation
Correlation
0.1
0.2
0.3
0.4
0.5
0.6
0.7
0.8
0.9
0.95
0.99
0.0
0.5
1.0
1.5
2.0
MARINE
DSI
GMI
GSN
HAT
MNM
PBL
SEY
YON
COASTAL
AMY
BKT_C
BKT_D
COI
CRI
PON_C
PON_D
RYO
TAP
MOUNTAIN
HLE_C
HLE_D
KZM
LLN
SNG
WLG
CONTINENTAL
DDR
JIN
KIS
KZD
LIN
LON
MKW
SDZ
UUM
WIS

Figure S14 The CH_4 and CO_2 synoptic variability at BKT ('C' for continuous measurements) and PON ('D' for discrete flask measurements) simulated from ZASIA (red dots) and REG (blue dots), in comparison with the observed CO_2 synoptic variability (black dots). For each station, synoptic variability is calculated as residuals from the smoothed fitting curve, and here for BKT and PON we extract and plot time series of the residuals for the year 2012 and 2009, respectively. The open circles indicate the synoptic events that are not realistically simulated by ZASIA, with a model-observation deviation (absolute value) beyond four times the average. Note the different model performance on CH_4 and CO_2 at the same station during the same period.

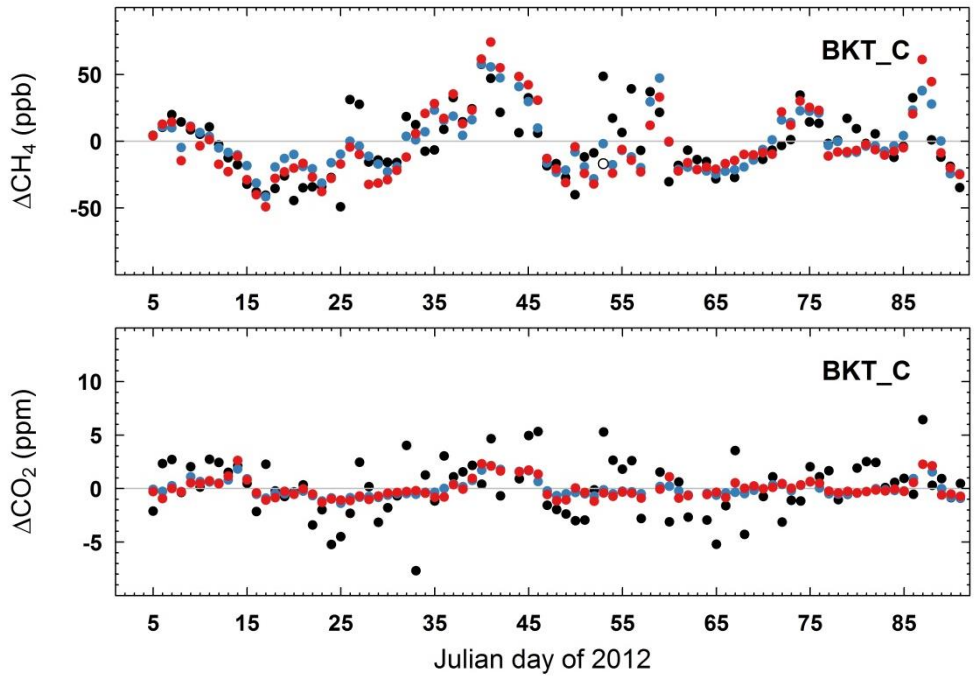

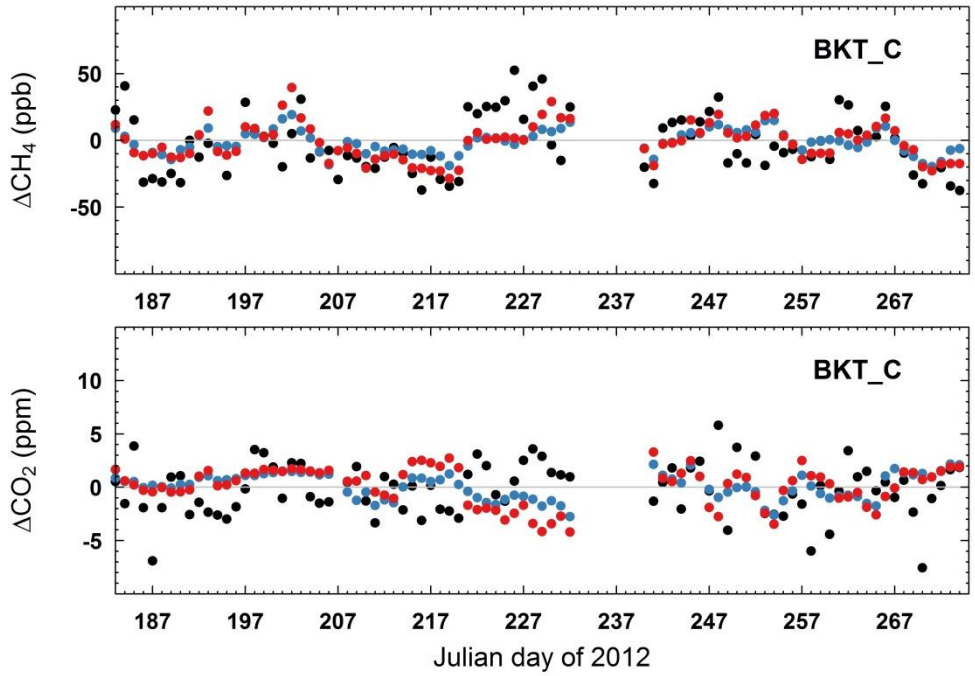
BKT_C
ΔCH4 (ppb)
50
0
-50
187
197
207
217
227
237
247
257
267
BKT_C
ΔCO2 (ppm)
10
5
0
-5
187
197
207
217
227
237
247
257
267
Julian day of 2012

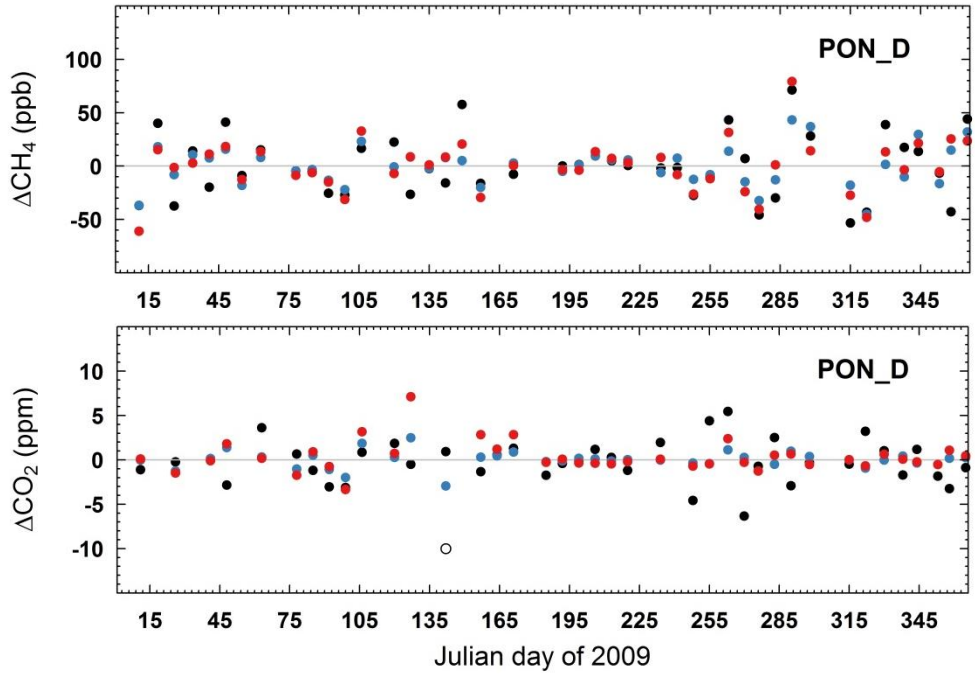
PON_D
ΔCH4 (ppb)
100
50
0
-50
15
45
75
105
135
165
195
225
255
285
315
345
PON_D
ΔCO2 (ppm)
10
5
0
-5
-10
15
45
75
105
135
165
195
225
255
285
315
345
Julian day of 2009

Reference

Kurokawa, J., Ohara, T., Morikawa, T., Hanayama, S., Janssens-Maenhout, G., Fukui, T., Kawashima, K. and Akimoto, H.: Emissions of air pollutants and greenhouse gases over Asian regions during 2000–2008: Regional Emission inventory in ASia (REAS) version 2, Atmos. Chem. Phys., 13(21), 11019–11058, doi:10.5194/acp-13-11019-2013, 2013.

Machida, T., Matsueda, H., Sawa, Y., Nakagawa, Y., Hirotani, K., Kondo, N., Goto, K., Nakazawa, T., Ishikawa, K. and Ogawa, T.: Worldwide Measurements of Atmospheric CO_2 and Other Trace Gas Species Using Commercial Airlines, J. Atmos. Ocean. Technol., 25(10), 1744–1754, doi:10.1175/2008JTECHA1082.1, 2008.